Over-the-Air Computation via Reconfigurable Intelligent Surface

Wenzhi Fang, *Student Member*, *IEEE*, Yuning Jiang, *Member*, *IEEE*, Yuanming Shi, *Senior Member*, *IEEE*, Yong Zhou, *Member*, *IEEE*, Wei Chen, *Senior Member*, *IEEE*, and Khaled B. Letaief, *Fellow*, *IEEE*

Abstract—Over-the-air computation (AirComp) is a disruptive technique for fast wireless data aggregation in Internet of Things (IoT) networks via exploiting the waveform superposition property of multiple-access channels. However, the performance of AirComp is bottlenecked by the worst channel condition among all links between the IoT devices and the access point. In this paper, a reconfigurable intelligent surface (RIS) assisted AirComp system is proposed to boost the received signal power and thus mitigate the performance bottleneck by reconfiguring the propagation channels. With an objective to minimize the AirComp distortion, we propose a joint design of AirComp transceivers and RIS phase-shifts, which however turns out to be a highly intractable non-convex programming problem. To this end, we develop a novel alternating minimization framework in conjunction with the successive convex approximation technique, which is proved to converge monotonically. To reduce the computational complexity, we transform the subproblem in each alternation as a smooth convex-concave saddle point problem, which is then tackled by proposing a Mirror-Prox method that only involves a sequence of closed-form updates. Simulations show that the computation time of the proposed algorithm can be two orders of magnitude smaller than that of the state-of-the-art algorithms, while achieving a similar distortion performance.

Index Terms—Over-the-air computation, reconfigurable intelligent surface, successive convex approximation, and Mirror-Prox method.

I. INTRODUCTION

Driven by the increasing advancement of wireless communication technologies and the decreasing manufacturing costs, Internet of Things (IoT) is expected to support ubiquitous connectivity and automatic transmission for billions of devices equipped with sensing and communication capabilities [2]. With limited spectrum resources, it is generally challenging to achieve efficient wireless data aggregation over a large volume of IoT devices, which is critical for unleashing the potential of the distributed sensory data. The conventional "transmit-then-compute" approach requires an access point (AP) to successfully receive the data from each IoT device and then compute a specific function (e.g., arithmetic mean) of the received data. This is, however, not spectrum-efficient, especially when the number of IoT devices is large. Fortunately, over-the-air computation (AirComp), which integrates the communication and computation processes, has the potential to achieve ultra-fast wireless data aggregation in IoT networks. This is accomplished by enabling the concurrent data transmissions from all IoT devices over the same radio channel and exploiting the waveform superposition property of multiple-access channels (MACs) at the AP [3], [4], yielding a revolutionary paradigm of "compute when communicate".

The study of AirComp can be traced back to the seminal work [5], which showed that a fast function computation can be achieved by enabling concurrent analog transmissions. There is a growing body of studies concentrated on the transceiver design for AirComp to enable efficient wireless data aggregation [6]–[10]. In particular, the authors in [6], [7] proposed optimal transmit power control strategies for AirComp in single-input single-output (SISO) wireless networks with energy-constrained IoT devices. The authors in [8] studied AirComp in multiple-input single-output (MISO) wireless networks, where a novel uniform-forcing transmit design was proposed to compensate the non-uniform channel fading among IoT devices. By integrating multiple-input multiple-output (MIMO) with AirComp, the authors in [9] and [10] investigated the transceiver design for multi-function computation and multi-modal sensing, respectively. By exploiting the property of AirComp, an efficient channel state information (CSI) estimation strategy was proposed in [10]. Meanwhile, the authors in [11] proposed a blind MIMO AirComp scheme to reduce the signaling overhead for CSI estimation. The authors in [12] proposed an automatic repeat request (ARQ) based communication scheme to reduce the overhead for CSI estimation and investigated the tradeoff between the computation rate and the transmission delay. AirComp was further extended to multi-hop wireless networks in [13], where the computation rate for multi-hop AirComp was derived. More recently, the authors in [14] derived a theoretical bound on the error of AirComp, where the channel correlation was taken into account. The authors in [15] considered the AirComp

Wenzhi Fang is with the School of Information Science and Technology, ShanghaiTech University, Shanghai 201210, China, also with the Shanghai Institute of Microsystem and Information Technology, Chinese Academy of Sciences, Shanghai 200050, China, and also with the University of Chinese Academy of Sciences, Beijing 100049, China (e-mail: fangwzh1@shanghaitech.edu.cn).

Yuning Jiang is with Automatic Control Laboratory, EPFL, Switzerland (e-mail: yuning.jiang@epfl.ch).

Yuanming Shi and Yong Zhou are with the School of Information Science and Technology, ShanghaiTech University, Shanghai 201210, China (e-mail: {shiym, zhouyong}@shanghaitech.edu.cn).

Wei Chen is with the Department of Electronic Engineering, Tsinghua University, Beijing 100084, China (e-mail: wchen@tsinghua.edu.cn).

Khaled B. Letaief is with the Department of Electronic and Computer Engineering, Hong Kong University of Science and Technology, Hong Kong, also with Peng Cheng Laboratory, Shenzhen, China (e-mail: eekhaled@ust.hk).

with correlated signals from different IoT devices, where both the theoretical optimal policy and low-complexity algorithm were developed. By calibrating the transmission timing of each IoT device, the synchronization issue of AirComp can be addressed. In case of non-strict synchronization, the authors in [16] proposed an efficient matched filtering and sampling scheme to facilitate misaligned AirComp. Besides, the authors in [17]–[19] exploited the advantages of AirComp to develop a fast model aggregation scheme to accelerate the convergence of federated learning. According to the aforementioned studies, AirComp requires the magnitudes of the signals to be aligned at the AP; thus, the performance of AirComp is bottlenecked by the worst channel between the IoT devices and the AP.

Reconfigurable intelligent surface (RIS) is an emerging technology, which has recently been proposed to tackle unfavorable channel conditions by reconfiguring the radio propagation environment [20]–[30]. An RIS is a man-made flat surface composed of many passive reflecting elements, each of which can independently shift the phase of the impinging waves in a controllable way [20], [21], thereby constructing a favorable wireless radio propagation environment. The authors in [22]–[24] demonstrated that RIS has the ability to significantly enhance the energy efficiency and spectral efficiency of wireless networks. Owing to the aforementioned features, RIS has been integrated with various wireless technologies, e.g., non-orthogonal multiple access (NOMA) [25], massive IoT device connectivity [26], massive MIMO [27], millimeter-wave communications [28], unmanned aerial vehicle communications [29], and wireless power transfer [30], to further enhance the network performance and promote emerging applications. Along with this line, to fully exploit the performance gain brought by RIS, various efficient channel estimation methods have been proposed for accurate CSI estimation, e.g., on-off state control [31], message-passing based algorithm [32], three-phase pilot-based framework [33], and anchor-assisted scheme [34]. To account for the imperfect CSI estimation, the authors in [35] and [36] studied the beamforming and phase-shift matrix design in RIS-assisted wireless networks by utilizing the worst-case optimization and stochastic optimization, respectively. Besides, the authors in [37] investigated the power minimization problem in MISO wireless networks with an uncertain cascaded device-RIS-AP channel, where both the worst-case optimization and stochastic optimization were considered.

To leverage the advantages of RIS for enhancing the quality of the worst channel between the IoT devices and the AP and in turn mitigating the performance bottleneck of AirComp, the authors in [1], [38] proposed an RIS-assisted AirComp system. In these two studies, the alternating semi-definite relaxation (SDR) algorithm and the alternating difference-of-convex (DC) algorithm were proposed to jointly optimize the receive beamforming vector at the AP and the phase-shift matrix at the RIS. However, both algorithms suffer from high computational complexity as they need to iteratively solve the semi-definite programming (SDP) problems. Moreover, the optimization of the phase-shift matrix in [1], [38] involves feasibility detection that cannot be accurately tackled

by the SDR and DC algorithms. Hence, both algorithms are not guaranteed to achieve monotonic convergence. This motivates us to develop a computationally efficient algorithm with convergence guarantee to achieve efficient wireless data aggregation in RIS-assisted AirComp systems.

A. Contributions

In this paper, we consider an RIS-assisted IoT network, where a multi-antenna AP aggregates the sensory data from multiple IoT devices by using AirComp with the assistance of an RIS. We evaluate the performance of AirComp in terms of the computation distortion, which is measured by the mean-squared-error (MSE). The main objective is to develop a low-complexity algorithm with convergence guarantee to minimize the MSE of RIS-assisted AirComp systems. To this end, it is necessary to jointly optimize the transmit scalars at the IoT devices, the receive beamforming vector and the denoising factor at the AP, and the phase-shifts at the RIS. The main contributions of this paper are summarized as follows:

- We formulate an MSE minimization problem for RIS-assisted AirComp systems, where the transmit scalars at the IoT devices, the receive beamforming vector and the denoising factor at the AP, and the phase-shift matrix at the RIS are jointly optimized. To tackle the scalability and convergence issues of existing studies, we transform the original problem into an equivalent min-max optimization problem. It turns out to be a highly intractable non-convex optimization problem due to the non-convex objective function and the coupled optimization variables.

- We propose a successive convex approximation (SCA) based alternating minimization (AlterMin) framework to alternately optimize the receive beamforming vector and the phase-shift vector. For each optimization problem in the alternating procedure, we iteratively construct a convex surrogate for the non-convex objective function by utilizing the SCA technique. We prove that the proposed framework is guaranteed to converge, which is a key difference from the existing studies on RIS-assisted AirComp. Besides, the number of iterations required to converge for AlterMin is small according to the simulations, which in turn reduces the computation cost. As the subproblem in each SCA iteration is a non-smooth convex problem, the conventional algorithms suffer from high computational complexity.

- As the objective function involves the pointwise maximum of affine functions, we equivalently transform the resulting non-smooth convex problem into a smooth convex-concave saddle point problem by using the primal-dual transformation. Subsequently, we adopt the Mirror-Prox method to solve the aforementioned saddle point problem and derive a closed-form expression for each update. As a result, the proposed Mirror-Prox based AlterMin SCA algorithm enjoys a very low computational complexity.

We conduct extensive simulations to demonstrate the monotonic convergence and the superior performance of the proposed algorithm for RIS-assisted AirComp systems. Results
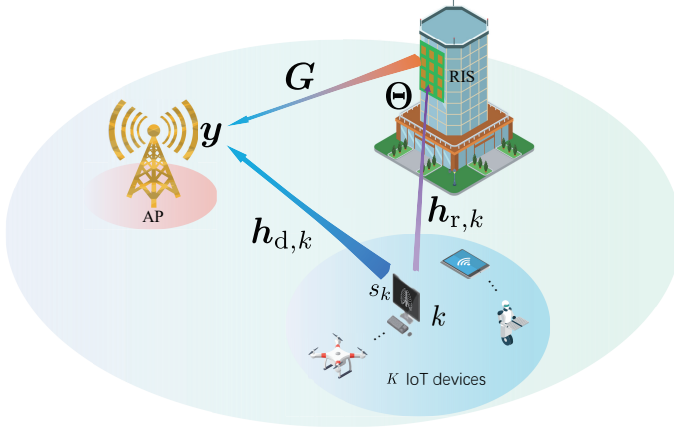
Fig. 1: Illustration of an RIS-assisted IoT network, where an AP aggregates the data from multiple IoT devices using AirComp.

will show that the computational time of the proposed algorithm can be two orders of magnitude smaller than that of the alternating SDR and alternating DC algorithms [1], [38], while achieving a similar data aggregation distortion performance in terms of MSE as these state-of-the-art algorithms. Moreover, the performance gain of the proposed algorithm in terms of the computation time increases when the dimensions of the system parameters (e.g., number of IoT devices, AP's antennas, and RIS's reflecting elements) become larger.

B. Organization and Notations

The reminder of this paper is organized as follows. Section II describes the system model and the problem formulation. Section III presents an AlterMin SCA framework for solving the formulated problem. Section IV provides the Mirror-Prox method to solve the subproblems in each SCA iteration. The performance of the proposed algorithm is illustrated in Section V. Finally, we conclude this paper in Section VI.

Notations: Matrices, vectors, and scalars are denoted by boldface upper-case, boldface lower-case, and lower-case letters, respectively. $(\cdot)^{\mathsf{H}}$, $(\cdot)^{\mathsf{T}}$, and $(\cdot)^{\dagger}$ stand for Hermitian transpose, transpose, and conjugate operators, respectively. $\|\cdot\|_1$, $\|\cdot\|$, and $\|\cdot\|_\infty$ denote the ℓ_1, ℓ_2, and ℓ_∞ norm operators, respectively. The operator $|\cdot|$ denotes the absolute value of a scalar number. $\Re[\cdot]$ and $\Im[\cdot]$ represent the real and imaginary parts of a complex matrix, vector, or scalar, respectively. $\mathbb{E}[\cdot]$ denotes the expectation of a random variable.

II. SYSTEM MODEL AND PROBLEM FORMULATION

In this section, we first present the system model of an RIS-assisted AirComp system and formulate an AirComp distortion minimization problem that requires the joint optimization of the transmit scalars at the IoT devices, the receive beamforming vector and the denoising factor at the AP, and the phase-shift matrix at the RIS. Subsequently, we discuss the limitations of the existing methods, which motivate us to reformulate an equivalent min-max optimization problem.

A. System Model

We consider the uplink transmission of an RIS-assisted single-cell IoT network consisting of K single-antenna IoT

devices, an AP with M antennas, and an RIS equipped with N passive reflecting elements, as shown in Fig. 1. We denote $\mathcal{K} = \{1, 2, \ldots, K\}$ as the index set of IoT devices. We consider the scenario that the AP, as a fusion center, is interested in receiving an aggregation (e.g., geometric mean, arithmetic mean) of the sensory data (e.g., temperature, humidity) from all IoT devices, rather than the individual data from each IoT device [9]. This process is generally referred to as wireless data aggregation in IoT networks. By integrating the computation and communication processes via exploiting the waveform superposition property of MACs, AirComp is adopted in this paper to achieve ultra-fast data aggregation by enabling concurrent transmissions from multiple IoT devices. We denote $z_k \in \mathbb{C}$ as the representative information-bearing data at IoT device k. Before transmission, IoT device k normalizes data z_k as information symbol $s_k \in \mathbb{C}$. Without loss of generality, we assume that $\{s_k\}_{k=1}^K$ have zero mean and unit power, and are independent of each other, i.e., $\mathbb{E}[s_k] = 0$, $\mathbb{E}[s_k s_k^*] = 1$, and $\mathbb{E}[s_k s_i^*] = 0$, $\forall k \neq i$ [6], [7]. The target function that the AP aims to recover is the summation of the data from all IoT devices, i.e.,

$$g = \sum_{k \in \mathcal{K}} s_k. \tag{1}$$

Based on the principle of AirComp, we assume that all IoT devices are synchronized and transmitted concurrently to the AP [9]. With universal frequency reuse, the signal received at the AP from all IoT devices is given by

$$\boldsymbol{y} = \sum_{k \in \mathcal{K}} (\boldsymbol{h}_{\mathrm{d},k} + \boldsymbol{G}\boldsymbol{\Theta}\boldsymbol{h}_{\mathrm{r},k}) w_k s_k + \boldsymbol{n}, \tag{2}$$

where $w_k \in \mathbb{C}$ denotes the transmit scalar of IoT device k, $\boldsymbol{\Theta} = \mathrm{diag}\{e^{j\theta_1}, e^{j\theta_2}, \ldots, e^{j\theta_N}\}$ denotes the diagonal phase-shift matrix of RIS with $0 \leq \theta_i < 2\pi$, $\forall i$, $\boldsymbol{h}_{\mathrm{d},k} \in \mathbb{C}^{M \times 1}$, $\boldsymbol{G} \in \mathbb{C}^{M \times N}$, and $\boldsymbol{h}_{\mathrm{r},k} \in \mathbb{C}^{N \times 1}$ denote the channel coefficients of the links from device k to the AP, from the RIS to the AP, and from device k to the RIS, respectively, and $\boldsymbol{n} \sim \mathcal{CN}(0, \sigma^2 \boldsymbol{I}_M)$ is the additive white Gaussian noise (AWGN) with zero mean and variance σ^2. Each device has a maximum transmit power, denoted as P. Hence, we have $|w_k|^2 \leq P, \forall k \in \mathcal{K}$. As various effective channel estimation methods have been proposed for RIS-assisted wireless networks [31]–[34], we assume that perfect CSI is available in our work, as in [22]–[30], [38]. Note that we only need the CSI of the direct link and the cascaded device-RIS-AP link, rather than that of the separated device-RIS and RIS-AP links. Besides, we consider block-fading channels, where the channel gain of each link remains invariant within one time slot but varies independently across different time slots. The estimated function at the AP is given by [17]

$$\hat{g} = \frac{1}{\sqrt{\eta}} \boldsymbol{m}^{\mathsf{H}} \boldsymbol{y}$$
$$= \frac{1}{\sqrt{\eta}} \boldsymbol{m}^{\mathsf{H}} \sum_{k \in \mathcal{K}} (\boldsymbol{h}_{\mathrm{d},k} + \boldsymbol{G}\boldsymbol{\Theta}\boldsymbol{h}_{\mathrm{r},k}) w_k s_k + \frac{1}{\sqrt{\eta}} \boldsymbol{m}^{\mathsf{H}} \boldsymbol{n}, \tag{3}$$

where $\boldsymbol{m} \in \mathbb{C}^M$ and η denote the receive beamforming vector and the denoising factor at the AP, respectively.

We adopt MSE to measure the distortion between the estimated function (i.e., $\hat{g}$) and the target function (i.e., g), which quantifies the performance of AirComp, given by

$$\mathsf{MSE}(\hat{g}, g) = \mathbb{E}\left(|\hat{g} - g|^2\right)$$
$$= \sum_{k \in \mathcal{K}} \left|\frac{1}{\sqrt{\eta}} \boldsymbol{m}^{\mathsf{H}}(\boldsymbol{h}_{\mathrm{d},k} + \boldsymbol{G}\boldsymbol{\Theta}\boldsymbol{h}_{\mathrm{r},k})w_k - 1\right|^2 + \frac{\sigma^2 \|\boldsymbol{m}\|^2}{\eta}. \quad (4)$$

Motivated by [8]–[10], [17], [38], [39], we adopt the following uniform-forcing design[1] to determine the transmit scalars of IoT devices

$$w_k^{\star} = \sqrt{\eta} \frac{(\boldsymbol{m}^{\mathsf{H}}(\boldsymbol{h}_{\mathrm{d},k} + \boldsymbol{G}\boldsymbol{\Theta}\boldsymbol{h}_{\mathrm{r},k}))^{\dagger}}{|\boldsymbol{m}^{\mathsf{H}}(\boldsymbol{h}_{\mathrm{d},k} + \boldsymbol{G}\boldsymbol{\Theta}\boldsymbol{h}_{\mathrm{r},k})|^2}, \ \forall \ k \in \mathcal{K}. \quad (5)$$

Due to the maximum transmit power constraint of IoT devices, i.e., $|w_k|^2 \le P$, η can be set as

$$\eta = P \min_{k \in \mathcal{K}} |\boldsymbol{m}^{\mathsf{H}}(\boldsymbol{h}_{\mathrm{d},k} + \boldsymbol{G}\boldsymbol{\Theta}\boldsymbol{h}_{\mathrm{r},k})|^2. \quad (6)$$

Therefore, the MSE at the AP can be further written as

$$\mathsf{MSE}(\boldsymbol{m}, \boldsymbol{\Theta}) = \frac{\|\boldsymbol{m}\|^2 \sigma^2}{P \min_{k \in \mathcal{K}} |\boldsymbol{m}^{\mathsf{H}}(\boldsymbol{h}_{\mathrm{d},k} + \boldsymbol{G}\boldsymbol{\Theta}\boldsymbol{h}_{\mathrm{r},k})|^2}. \quad (7)$$

The MSE given in (7) is determined by the transmit signal-to-noise ratio (SNR) $\frac{P}{\sigma^2}$, the receive beamforming vector $\boldsymbol{m}$ at the AP, and the composite channel coefficients $\boldsymbol{h}_{\mathrm{d},k} + \boldsymbol{G}\boldsymbol{\Theta}\boldsymbol{h}_{\mathrm{r},k}$, $\forall \ k$.

Remark 1. According to (7), the MSE of AirComp is bottlenecked by the worst channel between the IoT devices and the AP. Without RIS, i.e., $\boldsymbol{\Theta} = \boldsymbol{0}$, the channel quality is only determined by the direct link. In this case, we can only adjust the transmit power of IoT devices to tackle the detrimental effects of severe channel fading and path loss. With the assistance of RIS, the composite channel condition of each link (e.g., $\boldsymbol{h}_{\mathrm{d},k} + \boldsymbol{G}\boldsymbol{\Theta}\boldsymbol{h}_{\mathrm{r},k}$) can be adaptively adjusted by reconfiguring the phase-shift matrix $\boldsymbol{\Theta}$, which is able to enhance the channel quality of the link with the worse channel condition. As a result, the ability of RIS to reconfigure the propagation environment can be exploited to effectively mitigate the performance bottleneck of AirComp.

Our goal is to jointly optimize the phase-shift matrix $\boldsymbol{\Theta}$ and the receive beamforming vector $\boldsymbol{m}$ to minimize $\mathsf{MSE}(\boldsymbol{m}, \boldsymbol{\Theta})$ in (7). It is formulated as the following problem

$$\min_{\boldsymbol{m}, \boldsymbol{\Theta}} \frac{\|\boldsymbol{m}\|^2 \sigma^2}{P \min_{k \in \mathcal{K}} |\boldsymbol{m}^{\mathsf{H}}(\boldsymbol{h}_{\mathrm{d},k} + \boldsymbol{G}\boldsymbol{\Theta}\boldsymbol{h}_{\mathrm{r},k})|^2} \quad (8)$$
$$\text{s.t.} \ \ 0 \le \theta_i < 2\pi, \forall \ i.$$

Problem (8) can be equivalently expressed as

$$\min_{\boldsymbol{m}, \boldsymbol{\Theta}} \max_{k \in \mathcal{K}} \frac{\|\boldsymbol{m}\|^2 \sigma^2}{P |\boldsymbol{m}^{\mathsf{H}}(\boldsymbol{h}_{\mathrm{d},k} + \boldsymbol{G}\boldsymbol{\Theta}\boldsymbol{h}_{\mathrm{r},k})|^2} \quad (9)$$
$$\text{s.t.} \ \ 0 \le \theta_i < 2\pi, \forall \ i.$$

Since $\boldsymbol{\Theta}$ is a diagonal matrix and $\boldsymbol{h}_{\mathrm{r},k}$ is a vector, we rewrite $\boldsymbol{h}_{\mathrm{d},k} + \boldsymbol{G}\boldsymbol{\Theta}\boldsymbol{h}_{\mathrm{r},k}$ as $\boldsymbol{h}_{\mathrm{d},k} + \boldsymbol{G}\mathrm{diag}(\boldsymbol{h}_{\mathrm{r},k})\boldsymbol{v}$, where $\boldsymbol{v} =$

---

[1]It is clear that $\mathsf{MSE}(\hat{g}, g) \ge \frac{\sigma^2 \|\boldsymbol{m}\|^2}{\eta}$. Given $\boldsymbol{m}$ and $\boldsymbol{\Theta}$, the equality is achieved when $\{w_k\}_{k=1}^K$ are set according to (5), which enforces $\sum_{k \in \mathcal{K}} \left|\frac{1}{\sqrt{\eta}} \boldsymbol{m}^{\mathsf{H}}(\boldsymbol{h}_{\mathrm{d},k} + \boldsymbol{G}\boldsymbol{\Theta}\boldsymbol{h}_{\mathrm{r},k})w_k - 1\right|^2$ to be zero.

$[v_1, v_2, \ldots, v_N]$ with $v_i = e^{j\theta_i}$, $\forall \ i$. As $\frac{\sigma^2}{P}$ is a constant, Problem (9) is further equivalent to the following problem in the sense of having the same optimal solution

$$\min_{\boldsymbol{m}, \boldsymbol{v}} \max_k \frac{\|\boldsymbol{m}\|^2}{|\boldsymbol{m}^{\mathsf{H}}(\boldsymbol{h}_{\mathrm{d},k} + \boldsymbol{G}\mathrm{diag}(\boldsymbol{h}_{\mathrm{r},k})\boldsymbol{v})|^2} \quad (10)$$
$$\text{s.t.} \ \ |v_i| = 1, \forall \ i.$$

B. Limitations of State-of-the-Art Methods

Most of the existing studies [1], [25], [38] on the joint design in RIS-assisted wireless networks adopted the alternating SDR and alternating DC algorithms. According to [1], Problem (10) can be equivalently transformed to Problem (11) as follows

$$\min_{\boldsymbol{m}, \boldsymbol{v}} \|\boldsymbol{m}\|^2$$
$$\text{s.t.} \ \ |\boldsymbol{m}^{\mathsf{H}}(\boldsymbol{G}\mathrm{diag}(\boldsymbol{h}_{\mathrm{r},k})\boldsymbol{v} + \boldsymbol{h}_{\mathrm{d},k})|^2 \ge 1, \forall \ k, \quad (11)$$
$$|v_i| = 1, \ \forall \ i.$$

Problem (11) can be tackled by alternately solving the following two subproblems

$$\min_{\boldsymbol{m}} \|\boldsymbol{m}\|^2$$
$$\text{s.t.} \ \ |\boldsymbol{m}^{\mathsf{H}}\boldsymbol{h}_k^e|^2 \ge 1, \forall \ k, \quad (12)$$

and

$$\text{find} \ \boldsymbol{v}$$
$$\text{s.t.} \ \ |\boldsymbol{a}_k^{\mathsf{H}}\boldsymbol{v} + c_k|^2 \ge 1, \forall \ k, \quad (13)$$
$$|v_i|^2 = 1, \forall \ i,$$

where $\boldsymbol{h}_k^e = \boldsymbol{G}\mathrm{diag}(\boldsymbol{h}_{\mathrm{r},k})\boldsymbol{v} + \boldsymbol{h}_{\mathrm{d},k}$, $\boldsymbol{a}_k^{\mathsf{H}} = \boldsymbol{m}^{\mathsf{H}}\boldsymbol{G}\mathrm{diag}(\boldsymbol{h}_{\mathrm{r},k})$, and $c_k = \boldsymbol{m}^{\mathsf{H}}\boldsymbol{h}_{\mathrm{d},k}$. The two non-convex quadratically constrained quadratic programming (QCQP) problems, i.e., (12) and (13), were then converted into two SDP problems with rank-one constraint by using the matrix lifting approach. An intuitive solution is to apply the SDR technique to convexify the problems by directly dropping the rank-one constraint, yielding the alternating SDR algorithm [38]. As an alternative, based on the fact that the rank-one constraint of a positive definite matrix is equivalent to the zero-difference between the spectral norm and trace norm, a DC technique was proposed to tackle the rank-one constraint, yielding the alternating DC algorithm [1]. The existing studies that adopted the aforementioned frameworks suffer from two limitations, i.e., non-guaranteed convergence and high computation complexity. Specifically, the optimization of phase-shift vector $\boldsymbol{v}$ involves a feasibility detection problem, i.e., (13). According to the analysis in [40], both the alternating SDR and alternating DC algorithms are not guaranteed to converge. Besides, AirComp is expected to support wireless data aggregation in high-density IoT networks, where the number of IoT devices would be large. However, the aforementioned state-of-the-art methods, i.e., alternating DC and alternating SDR algorithms, are not scalable because of their high computational complexity. Especially for the alternating DC algorithm, a series of SDP problems generated by the SCA technique need to be solved by the standard interior-point method [41] at each alternating iteration. The computation time consumption would be an unaffordable

burden when the aforementioned algorithms are applied to solve large-scale optimization problems. The limitations of the existing studies motivate us to develop a low-complexity algorithm with a theoretical convergence guarantee for RIS-assisted AirComp systems.

C. Problem Transformation

To mitigate the aforementioned limitations, in this subsection, we reformulate Problem (10) as a min-max optimization problem, which is presented in the following proposition.

Proposition 1. Problem (10) is equivalent to the following min-max QCQP problem in the sense of optimal solution:

$$\min_{\boldsymbol{m},\boldsymbol{v}} \max_{k} \left\{ -|\boldsymbol{m}^{\mathsf{H}}(\boldsymbol{h}_{\mathrm{d},k} + \boldsymbol{G}\mathrm{diag}(\boldsymbol{h}_{\mathrm{r},k})\boldsymbol{v})|^2 \right\}$$
$$\text{s.t.} \quad |v_i| = 1, \forall\, i, \tag{14}$$
$$\|\boldsymbol{m}\|^2 = 1.$$

Proof. Please refer to Appendix A. □

As can be observed from (14), both optimization variables $\boldsymbol{m}$ and $\boldsymbol{v}$ are involved in the objective function. This transformation enables us to eliminate the feasibility detection problem as in [1], and allows us to exploit the monotonicity of the objective function during alternating minimization. Problem (14) is still a challenging non-convex optimization problem. Specifically, solving Problem (14) faces the following three challenges. First, the optimization variables $\boldsymbol{v}$ and $\boldsymbol{m}$ are coupled in the objective function. Second, the unit-modulus constraint on v_i, $\forall\, i$ and the unit receive power constraint on $\boldsymbol{m}$ are non-convex. Third, the pointwise maximum of quadratic terms, i.e., the objective function, is non-convex and non-smooth. To tackle these issues, we shall propose an alternating minimization method in conjunction with SCA to solve Problem (14) in the following section.

III. PROPOSED ALTERMIN SCA FRAMEWORK

In this section, we propose an alternating minimization method to alternately optimize the receive beamforming vector $\boldsymbol{m}$ and the phase-shift vector $\boldsymbol{v}$, resulting in two non-convex subproblems with respect to $\boldsymbol{m}$ and $\boldsymbol{v}$, respectively. We then construct convex approximations for the two yielded subproblems by using SCA.

A. Phase-Shift Vector Optimization

When the receive beamforming vector $\boldsymbol{m}$ is fixed, Problem (14) is reduced to the following subproblem that requires the optimization of phase-shift vector $\boldsymbol{v}$

$$\min_{\boldsymbol{v}} \max_{k} \left\{ -|\boldsymbol{m}^{\mathsf{H}}(\boldsymbol{h}_{\mathrm{d},k} + \boldsymbol{G}\mathrm{diag}(\boldsymbol{h}_{\mathrm{r},k})\boldsymbol{v})|^2 \right\}$$
$$\text{s.t.} \quad |v_i| = 1, \forall\, i = 1, \dots, N. \tag{15}$$

By denoting $c_k = \boldsymbol{m}^{\mathsf{H}}\boldsymbol{h}_{\mathrm{d},k}$ and $\boldsymbol{a}_k^{\mathsf{H}} = \boldsymbol{m}^{\mathsf{H}}\boldsymbol{G}\mathrm{diag}(\boldsymbol{h}_{\mathrm{r},k})$, Problem (15) can be rewritten as

$$\min_{\boldsymbol{v}} \max_{k} \left\{ -|c_k + \boldsymbol{a}_k^{\mathsf{H}}\boldsymbol{v}|^2 \right\}$$
$$\text{s.t.} \quad |v_i| = 1, \forall\, i. \tag{16}$$

For simplicity of algorithm design, we further convert Problem (16) from the complex domain to the real domain. By denoting $\tilde{\boldsymbol{v}} = [\Re\{\boldsymbol{v}\}^{\mathsf{T}}, \Im\{\boldsymbol{v}\}^{\mathsf{T}}]^{\mathsf{T}} \in \mathbb{R}^{2N}$, we obtain the following problem

$$\min_{\tilde{\boldsymbol{v}}} \max_{k} \left\{ \tilde{\boldsymbol{v}}^{\mathsf{T}}\tilde{\mathbf{A}}_k\tilde{\boldsymbol{v}} - 2\tilde{\boldsymbol{v}}^{\mathsf{T}}\boldsymbol{b}_k - |c_k|^2 \right\}$$
$$\text{s.t.} \quad \tilde{v}_i^2 + \tilde{v}_{i+N}^2 = 1, \forall\, i, \tag{17}$$

where $\boldsymbol{b}_k = [\Re\{c_k\boldsymbol{a}_k\}^{\mathsf{T}}, \Im\{c_k\boldsymbol{a}_k\}^{\mathsf{T}}]^{\mathsf{T}}$ and

$$\tilde{\mathbf{A}}_k = \begin{bmatrix} \Re\left\{-\boldsymbol{a}_k\boldsymbol{a}_k^{\mathsf{H}}\right\} & -\Im\left\{-\boldsymbol{a}_k\boldsymbol{a}_k^{\mathsf{H}}\right\} \\ \Im\left\{-\boldsymbol{a}_k\boldsymbol{a}_k^{\mathsf{H}}\right\} & \Re\left\{-\boldsymbol{a}_k\boldsymbol{a}_k^{\mathsf{H}}\right\} \end{bmatrix}.$$

Problem (17) aims to minimize the pointwise maximum of concave quadratic terms. Solving Problem (17) is challenging due to the non-convex constraints and the non-convex objective function. In the following, we tackle the non-convex constraint by utilizing the convex relaxation technique. Specifically, we relax the unit modulus constraint to $\tilde{\boldsymbol{v}} \in \mathcal{V}$, where $\mathcal{V} = \{\tilde{\boldsymbol{v}} \mid \tilde{v}_i^2 + \tilde{v}_{i+N}^2 \leq 1, \forall\, i = 1, \dots, N\}$, yielding the following relaxed problem

$$\min_{\tilde{\boldsymbol{v}}} \max_{k} \left\{ \tilde{\boldsymbol{v}}^{\mathsf{T}}\tilde{\mathbf{A}}_k\tilde{\boldsymbol{v}} - 2\tilde{\boldsymbol{v}}^{\mathsf{T}}\boldsymbol{b}_k - |c_k|^2 \right\}$$
$$\text{s.t.} \quad \tilde{\boldsymbol{v}} \in \mathcal{V}. \tag{18}$$

On the other hand, the SCA technique is applied to tackle the non-convexity of the objective function $\max_k \left\{ \tilde{\boldsymbol{v}}^{\mathsf{T}}\tilde{\mathbf{A}}_k\tilde{\boldsymbol{v}} - 2\tilde{\boldsymbol{v}}^{\mathsf{T}}\boldsymbol{b}_k - |c_k|^2 \right\}$. In particular, due to the concavity of $\{\tilde{\boldsymbol{v}}^{\mathsf{T}}\tilde{\mathbf{A}}_k\tilde{\boldsymbol{v}} - 2\tilde{\boldsymbol{v}}^{\mathsf{T}}\boldsymbol{b}_k - |c_k|^2\}$, we construct its linear upper bound based on the first-order Taylor approximation as

$$\tilde{\boldsymbol{v}}^{\mathsf{T}}\tilde{\mathbf{A}}_k\tilde{\boldsymbol{v}} - 2\tilde{\boldsymbol{v}}^{\mathsf{T}}\boldsymbol{b}_k - |c_k|^2 \leq \left(\mathbf{p}_k^{(n)}\right)^{\mathsf{T}}\tilde{\boldsymbol{v}} + q_k^{(n)},$$

where $\mathbf{p}_k^{(n)} = 2(\tilde{\mathbf{A}}_k\tilde{\boldsymbol{v}}^{(n)} - \boldsymbol{b}_k)$, $q_k^{(n)} = -(\tilde{\boldsymbol{v}}^{(n)})^{\mathsf{T}}\tilde{\mathbf{A}}_k\tilde{\boldsymbol{v}}^{(n)} - |c_k|^2$, and $\tilde{\boldsymbol{v}}^{(n)}$ is the solution obtained at the n-th iteration. As a result, we have

$$\max_{k} \left\{ \tilde{\boldsymbol{v}}^{\mathsf{T}}\tilde{\mathbf{A}}_k\tilde{\boldsymbol{v}} - 2\tilde{\boldsymbol{v}}^{\mathsf{T}}\boldsymbol{b}_k - |c_k|^2 \right\} \leq \max_{k} \left\{ \left(\mathbf{p}_k^{(n)}\right)^{\mathsf{T}}\tilde{\boldsymbol{v}} + q_k^{(n)} \right\}. \tag{19}$$

Therefore, at the $(n+1)$-th iteration, we can replace the non-convex objective function in Problem (18) by its convex surrogate $\max_k \left\{ \left(\mathbf{p}_k^{(n)}\right)^{\mathsf{T}}\tilde{\boldsymbol{v}} + q_k^{(n)} \right\}$. Specifically, at the $(n+1)$-th iteration, Problem (18) is approximated by the following subproblem

$$\min_{\tilde{\boldsymbol{v}}} \max_{k} \left(\mathbf{p}_k^{(n)}\right)^{\mathsf{T}}\tilde{\boldsymbol{v}} + q_k^{(n)}$$
$$\text{s.t.} \quad \tilde{\boldsymbol{v}} \in \mathcal{V}. \tag{20}$$

To efficiently solve Problem (18), we resort to iteratively solve its non-smooth convex approximation problem (20).

B. Receive Beamforming Vector Optimization

When the phase-shift vector $\boldsymbol{v}$ is fixed, (14) can be formulated as an optimization problem with respect to the receive beamforming vector $\boldsymbol{m}$ as follows

$$\min_{\boldsymbol{m}} \max_{k} \left\{ -|\boldsymbol{m}^{\mathsf{H}}(\boldsymbol{h}_{\mathrm{d},k} + \boldsymbol{G}\mathrm{diag}(\boldsymbol{h}_{\mathrm{r},k})\boldsymbol{v})|^2 \right\}$$
$$\text{s.t.} \quad \|\boldsymbol{m}\|^2 = 1. \tag{21}$$

By denoting $\boldsymbol{h}_k = \boldsymbol{h}_{\mathrm{d},k} + \boldsymbol{G}\mathrm{diag}(\boldsymbol{h}_{\mathrm{r},k})\boldsymbol{v}$, (21) can be represented as

$$\min_{\boldsymbol{m}} \max_{k} \ \left\{-|\boldsymbol{m}^{\mathsf{H}}\boldsymbol{h}_k|^2\right\} \tag{22}$$
$$\text{s.t. } \|\boldsymbol{m}\|^2 = 1.$$

The constraint in (22) is non-convex. According to [42], Problem (22) is equivalent to the following problem

$$\min_{\boldsymbol{m}} \max_{k} \ \left\{-|\boldsymbol{m}^{\mathsf{H}}\boldsymbol{h}_k|^2\right\} \tag{23}$$
$$\text{s.t. } \|\boldsymbol{m}\|^2 \leq 1.$$

This is because that the constraint should be met with equality at the optimal point for Problem (23). Otherwise, $\boldsymbol{m}$ could be scaled up to reduce the objective value, thereby contradicting the optimality. By defining $\tilde{\boldsymbol{m}} = [\Re\{\boldsymbol{m}\}^{\mathsf{T}}, \Im\{\boldsymbol{m}\}^{\mathsf{T}}]^{\mathsf{T}} \in \mathbb{R}^{2M}$, we convert Problem (23) from the complex domain to the real domain to facilitate the algorithm design

$$\min_{\tilde{\boldsymbol{m}}} \max_{k} \ \tilde{\boldsymbol{m}}^{\mathsf{T}}\tilde{\mathbf{H}}_k\tilde{\boldsymbol{m}} \tag{24}$$
$$\text{s.t. } \tilde{\boldsymbol{m}} \in \mathcal{M},$$

where $\mathcal{M} = \{\tilde{\boldsymbol{m}} \mid \|\tilde{\boldsymbol{m}}\|^2 \leq 1\}$ and

$$\tilde{\mathbf{H}}_k = \begin{bmatrix} \Re\left\{-\boldsymbol{h}_k\boldsymbol{h}_k^{\mathsf{H}}\right\} & -\Im\left\{-\boldsymbol{h}_k\boldsymbol{h}_k^{\mathsf{H}}\right\} \\ \Im\left\{-\boldsymbol{h}_k\boldsymbol{h}_k^{\mathsf{H}}\right\} & \Re\left\{-\boldsymbol{h}_k\boldsymbol{h}_k^{\mathsf{H}}\right\} \end{bmatrix}.$$

To tackle the non-convexity of the objective function of Problem (24), we shall apply SCA to construct its local convex approximation. Due to the similar structure of Problem (18) and Problem (24), the derivation here is similar to that presented in Section III-A. For completeness, we sketch the main procedures for solving Problem (24). Starting from an initial point $\tilde{\boldsymbol{m}}^{(0)} \in \mathcal{M}$, SCA is applied to generate a sequence of solutions $\{\tilde{\boldsymbol{m}}^{(n)}\}$ as follows. With the approximated solution $\tilde{\boldsymbol{m}}^{(n)}$ obtained at the n-th iteration, the concave quadratic function $\tilde{\boldsymbol{m}}^{\mathsf{T}}\tilde{\mathbf{H}}_k\tilde{\boldsymbol{m}}$ can be upper bounded by its linear majorization. Specifically, we have the following inequality

$$\tilde{\boldsymbol{m}}^{\mathsf{T}}\tilde{\mathbf{H}}_k\tilde{\boldsymbol{m}} \leq (2\tilde{\mathbf{H}}_k\tilde{\boldsymbol{m}}^{(n)})^{\mathsf{T}}\tilde{\boldsymbol{m}} - (\tilde{\boldsymbol{m}}^{(n)})^{\mathsf{T}}\tilde{\mathbf{H}}_k\tilde{\boldsymbol{m}}^{(n)}.$$

By denoting $\bar{\mathbf{p}}_k^{(n)} = 2\tilde{\mathbf{H}}_k\tilde{\boldsymbol{m}}^{(n)}$ and $\bar{q}_k^{(n)} = -(\tilde{\boldsymbol{m}}^{(n)})^{\mathsf{T}}\tilde{\mathbf{H}}_k\tilde{\boldsymbol{m}}^{(n)}$, we have

$$\max_{k} \ \left\{\tilde{\boldsymbol{m}}^{\mathsf{T}}\tilde{\mathbf{H}}_k\tilde{\boldsymbol{m}}\right\} \leq \max_{k} \ \left\{\bar{\mathbf{p}}_k^{(n)\mathsf{T}}\tilde{\boldsymbol{m}} + \bar{q}_k^{(n)}\right\}. \tag{25}$$

Then, $\tilde{\boldsymbol{m}}^{(n+1)}$ can be obtained by solving the following non-smooth convex approximation problem

$$\min_{\tilde{\boldsymbol{m}}} \max_{k} \ \bar{\mathbf{p}}_k^{(n)\mathsf{T}}\tilde{\boldsymbol{m}} + \bar{q}_k^{(n)} \tag{26}$$
$$\text{s.t. } \tilde{\boldsymbol{m}} \in \mathcal{M}.$$

C. Convergence Analysis

We recall that Problem (14) is decomposed into two Problems (18) and (24) with respect $\tilde{\boldsymbol{v}}$ and $\tilde{\boldsymbol{m}}$, respectively, which are then alternately solved by using SCA. Finally, we project $\tilde{\boldsymbol{v}}$ to $\mathcal{V}_1 = \{\tilde{\boldsymbol{v}} \mid \tilde{v}_i^2 + \tilde{v}_{i+N}^2 = 1, \forall \ i\}$, so as to compensate the relaxation on $\tilde{\boldsymbol{v}}$. The overall AlterMin SCA algorithm for solving Problem (14) is summarized in Algorithm 1. The convergence of Algorithm 1 is presented in the following proposition.

Algorithm 1: AlterMin SCA for Problem (14)

Input: Initial point $\tilde{\boldsymbol{v}}_{(0)}^{(0)}$, $\tilde{\boldsymbol{m}}_{(0)}^{(0)}$ and threshold ϵ;

1 Set: $l = 0$;
2 **repeat**
3 $\quad$ Set: $n = 0$;
4 $\quad$ **repeat**
5 $\quad\quad$ Update $\tilde{\boldsymbol{v}}_{(l)}^{(n+1)}$ by solving Problem (20);
6 $\quad\quad$ $n \leftarrow n + 1$;
7 $\quad$ **until** *the decrease of objective value of*
$\quad\quad \tilde{\boldsymbol{v}}^{\mathsf{T}}\tilde{\mathbf{A}}_k\tilde{\boldsymbol{v}} - 2\tilde{\boldsymbol{v}}^{\mathsf{T}}\boldsymbol{b}_k - |c_k|^2$ *less than ϵ;*
8 $\quad$ Set: $\tilde{\boldsymbol{v}}_{(l+1)}^{(0)} = \tilde{\boldsymbol{v}}_{(l)}^{(n)}$;
9 $\quad$ Set: $n = 0$;
10 $\quad$ **repeat**
11 $\quad\quad$ Update $\tilde{\boldsymbol{m}}_{(l)}^{(n+1)}$ by solving Problem (26);
12 $\quad\quad$ $n \leftarrow n + 1$;
13 $\quad$ **until** *the decrease of objective value of $\tilde{\boldsymbol{m}}^{\mathsf{T}}\tilde{\mathbf{H}}_k\tilde{\boldsymbol{m}}$*
$\quad\quad$ *less than ϵ;*
14 $\quad$ Set: $\tilde{\boldsymbol{m}}_{(l+1)}^{(0)} = \tilde{\boldsymbol{m}}_{(l)}^{(n)}$;
15 $\quad$ $l \leftarrow l + 1$;
16 **until** *the decrease of objective value*
$\quad \left\{-|\boldsymbol{m}^{\mathsf{H}}(\boldsymbol{h}_{\mathrm{d},k} + \boldsymbol{G}\mathrm{diag}(\boldsymbol{h}_{\mathrm{r},k})\boldsymbol{v})|^2\right\}$ *less than ϵ;*
17 Project $\tilde{\boldsymbol{v}}$ to set $\mathcal{V}_1$.

Proposition 2. The convergence property of Algorithm 1 consists of two parts:

i) In the inner loop (Steps 4-7 and Steps 10-13), i.e., SCA iteration, the objective values of Problems (18) and (24) achieved by sequences $\{\tilde{\boldsymbol{v}}_{(l)}^{(n)}\}_{n=0}^{\infty}$ and $\{\tilde{\boldsymbol{m}}_{(l)}^{(n)}\}_{n=0}^{\infty}$ establish non-increasing convergent sequences;

ii) In the outer loop (Steps 2-16), i.e., alternating minimization iteration, the objective value of Problem (14) achieved by the sequence $\{\tilde{\boldsymbol{v}}_{(l)}^{(0)}, \tilde{\boldsymbol{m}}_{(l)}^{(0)}\}_{l=0}^{\infty}$ establish a non-increasing convergent sequence.

Proof. Please refer to Appendix B. $\quad\square$

D. Algorithm Discussion

To efficiently solve Problem (14), we still need to design an efficient algorithm to solve Problem (20) and Problem (26). However, the objective function $\max_k\{(\mathbf{p}_k^{(n)})^{\mathsf{T}}\tilde{\boldsymbol{v}} + q_k^{(n)}\}$ of Problem (20) is convex but non-smooth. Intuitively, the subgradient algorithm as a first-order method can be applied. However, it requires $\mathcal{O}\left(\frac{1}{\epsilon^2}\right)$ iterations to attain an ϵ-optimal solution [43]. The Nesterov's smoothing technique in conjunction with the majorization-minimization (MM) method [44], [45] can be adopted to solve Problem (20). It attains an ϵ-optimal solution within $\mathcal{O}\left(\frac{1}{\epsilon^2}\right)$ iterations when a quadratic function is constructed in the majorization step [46]. In addition, by introducing an auxiliary variable r, Problem (20) can be equivalently formulated as the following convex QCQP

problem

$$\min_{\tilde{\boldsymbol{v}},r} \quad r$$

$$\text{s.t.} \quad \left(\mathbf{p}_k^{(n)}\right)^\mathsf{T} \tilde{\boldsymbol{v}} + q_k^{(n)} - r \leq 0, \forall\, k, \tag{27}$$

$$\tilde{\boldsymbol{v}} \in \mathcal{V},\ r \in \mathbb{R}.$$

Problem (27) can be solved by using the interior-point method [41], which attains an ϵ-optimal solution with only $\mathcal{O}\left(\sqrt{N+K}\log\frac{2(N+K)}{\epsilon}\right)$ iterations. However, the time complexity of each iteration is $\mathcal{O}\left((N+K)N^2 + N^3\right)$ [41]. As Problem (20) and Problem (26) have a similar form, the above analysis also applies to Problem (26). Hence, all of the aforementioned algorithms cannot efficiently solve our problem when the number of optimization variables is large. This motivates us to exploit the underlying structure of Problems (20) and (26) to develop a highly efficient algorithm with a fast convergence rate and low iteration cost in the following section.

IV. MIRROR-PROX FOR NON-SMOOTH CONVEX PROBLEMS

In this section, we aim to develop a low-complexity algorithm to solve the non-smooth convex problems (20) and (26). We equivalently convert Problems (20) and (26) to the smooth convex-concave saddle point problems by using the primal-dual transformation, and then propose to use the Mirror-Prox method [47] to solve the resulting problems.

A. Mirror-Prox Method for Non-smooth Convex Problem (20)

1) Smooth Saddle Point Problem Formulation: The objective function of Problem (20) is pointwise maximum of affine functions. We equivalently convert non-smooth problem (20) to a smooth convex-concave saddle point problem in Lemma 1.

Lemma 1. (Primal-Dual Transformation) The non-smooth convex problem (20) is equivalent to the following smooth convex-concave saddle point problem

$$\min_{\tilde{\boldsymbol{v}}} \max_{\boldsymbol{y}} \quad \left(\mathbf{P}^{(n)}\tilde{\boldsymbol{v}} + \mathbf{q}^{(n)}\right)^\mathsf{T} \boldsymbol{y} \tag{28}$$

$$\text{s.t.} \quad \tilde{\boldsymbol{v}} \in \mathcal{V},\ \boldsymbol{y} \in \mathcal{Y},$$

where $\mathbf{P}^{(n)} = \left[\mathbf{p}_1^{(n)}, \mathbf{p}_2^{(n)}, \ldots, \mathbf{p}_K^{(n)}\right]^\mathsf{T}$, $\mathbf{q}^{(n)} = \left[q_1^{(n)}, q_2^{(n)}, \ldots, q_K^{(n)}\right]^\mathsf{T}$, and $\boldsymbol{y}$ is the Lagrangian dual variable with set $\mathcal{Y} = \{\boldsymbol{y}|\boldsymbol{y} \geq \mathbf{0}, \mathbf{1}^\mathsf{T}\boldsymbol{y} = 1, \boldsymbol{y} \in \mathcal{R}^K\}$ being the feasible domain.

Proof. Please refer to Appendix C. □

Different from the Nesterov's smoothing technique discussed in Section III-D, which relies on the smoothness parameter to balance the tradeoff between approximation accuracy and computation efficiency, our proposed method is parameter-free and the resulting smooth saddle point problem (28) is equivalent to the non-smooth problem (20) rather than an approximation. By denoting $\psi^{(n)}(\tilde{\boldsymbol{v}}, \boldsymbol{y}) := \left(\mathbf{P}^{(n)}\tilde{\boldsymbol{v}} + \mathbf{q}^{(n)}\right)^\mathsf{T}\boldsymbol{y}$,

solving non-smooth convex problem (28) is equivalent to finding a saddle point for the smooth convex-concave function $\psi^{(n)}(\tilde{\boldsymbol{v}}, \boldsymbol{y})$ under $\mathcal{V} \times \mathcal{Y}$.

2) First-Order Optimality Condition: By denoting $(\tilde{\boldsymbol{v}}^*, \mathbf{y}^*)$ as the saddle point of $\psi^{(n)}(\tilde{\boldsymbol{v}}, \mathbf{y})$, we have

$$\psi^{(n)}\left(\tilde{\boldsymbol{v}}^*, \boldsymbol{y}\right) \leq \psi^{(n)}\left(\tilde{\boldsymbol{v}}^*, \boldsymbol{y}^*\right) \leq \psi^{(n)}\left(\tilde{\boldsymbol{v}}, \boldsymbol{y}^*\right), \forall(\tilde{\boldsymbol{v}}, \boldsymbol{y}) \in \mathcal{V} \times \mathcal{Y}. \tag{29}$$

The first-order optimality condition [48] of a saddle point for $\psi^{(n)}(\tilde{\boldsymbol{v}}, \boldsymbol{y})$ is given by

$$\begin{cases} \nabla_{\tilde{\boldsymbol{v}}}\psi^{(n)}\left(\tilde{\boldsymbol{v}}^*, \boldsymbol{y}^*\right)\left(\tilde{\boldsymbol{v}} - \tilde{\boldsymbol{v}}^*\right) \geq 0, \\ -\nabla_{\boldsymbol{y}}\psi^{(n)}\left(\tilde{\boldsymbol{v}}^*, \boldsymbol{y}^*\right)\left(\boldsymbol{y} - \boldsymbol{y}^*\right) \geq 0, \end{cases} \forall\, (\tilde{\boldsymbol{v}}, \boldsymbol{y}) \in \mathcal{V} \times \mathcal{Y}. \tag{30}$$

By denoting $\boldsymbol{z} = \left[\tilde{\boldsymbol{v}}^\mathsf{T}, \boldsymbol{y}^\mathsf{T}\right]^\mathsf{T}$ and

$$\mathbf{F}(\boldsymbol{z}) := \begin{bmatrix} \nabla_{\tilde{\boldsymbol{v}}}\psi^{(n)}(\tilde{\boldsymbol{v}}, \boldsymbol{y}) \\ -\nabla_{\boldsymbol{y}}\psi^{(n)}(\tilde{\boldsymbol{v}}, \boldsymbol{y}) \end{bmatrix} = \begin{bmatrix} (\mathbf{P}^{(n)})^\mathsf{T}\boldsymbol{y} \\ -\left(\mathbf{P}^{(n)}\tilde{\boldsymbol{v}} + \mathbf{q}^{(n)}\right) \end{bmatrix},$$

the first-order optimality condition (30) can be rewritten in a more compact form as follows

$$\mathbf{F}\left(\boldsymbol{z}^*\right)^\mathsf{T}\left(\boldsymbol{z} - \boldsymbol{z}^*\right) \geq 0, \forall\, \boldsymbol{z} \in \mathcal{V} \times \mathcal{Y}. \tag{31}$$

Lemma 2. The operator $\mathbf{F}(\boldsymbol{z})$ is monotone and L-Lipschitz continuous on space $\mathcal{V} \times \mathcal{Y}$, where $\mathcal{V}$ is endowed with ℓ_2 norm, $\mathcal{Y}$ is endowed with ℓ_1 norm, and the Lipschitz parameter $L = \max_k\{\|\mathbf{p}_k^{(n)}\|\}$.

Proof. Please refer to Appendix D. □

Given the above, Problem (28) is equivalent to the following variational inequality problem with monotone and L-Lipschitz continuous operator:

$$\text{find} \quad \boldsymbol{z}^*$$

$$\text{s.t.} \quad \mathbf{F}\left(\boldsymbol{z}^*\right)^\mathsf{T}\left(\boldsymbol{z} - \boldsymbol{z}^*\right) \geq 0, \forall\, \boldsymbol{z} \in \mathcal{V} \times \mathcal{Y}, \tag{32}$$

$$\boldsymbol{z}^* \in \mathcal{V} \times \mathcal{Y}.$$

Remark 2. $\mathbf{F}(\boldsymbol{z})$ can be regarded as a gradient-type vector field on space $\mathcal{V} \times \mathcal{Y}$. The variational inequality $\mathbf{F}\left(\boldsymbol{z}^*\right)^\mathsf{T}\left(\boldsymbol{z} - \boldsymbol{z}^*\right) \geq 0$ is similar to the first-order optimality condition for convex constrained problems, where $\mathbf{F}$ resembles the gradient or subgradient. Hence, an intuitive solution is to employ the generalized projected gradient method [49] to solve Problem (32). However, the classical gradient-type algorithm cannot monitor the local geometry in the non-Euclidean space [50], thereby, weakening the algorithm performance. This motivates the Mirror-Prox method, which we shall present as follows.

3) Mirror-Prox Method: The Mirror-Prox method was firstly proposed in [47] for solving the Lipschitz continuous variational inequality problem with convergence rate $\mathcal{O}\left(\frac{1}{t}\right)$. The effectiveness of the Mirror-Prox method was demonstrated in [51] by developing a fast algorithm for multicast beamforming and antenna selection in massive MIMO wireless networks. Specifically, at each iteration, the Mirror-Prox method updates $\boldsymbol{z}$ through the following two steps

$$\boldsymbol{z}_{t+1}' = \arg\min_{\boldsymbol{z} \in \mathcal{V} \times \mathcal{Y}} \left\{D\left(\boldsymbol{z}, \boldsymbol{z}_t\right) + \left\langle\gamma\mathbf{F}\left(\boldsymbol{z}_t\right), \boldsymbol{z}\right\rangle\right\}, \tag{33a}$$

$$\boldsymbol{z}_{t+1} = \arg\min_{\boldsymbol{z} \in \mathcal{V} \times \mathcal{Y}} \left\{D\left(\boldsymbol{z}, \boldsymbol{z}_t\right) + \left\langle\gamma\mathbf{F}\left(\boldsymbol{z}_{t+1}'\right), \boldsymbol{z}\right\rangle\right\}, \tag{33b}$$
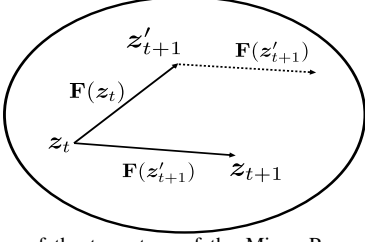
Fig. 2: Illustration of the two steps of the Mirror-Prox method in the t-th iteration.

where $D(\boldsymbol{z}, \boldsymbol{z}_t)$ denotes the Bregman distance and γ is a parameter that is determined by the Lipschitz parameter of $\mathbf{F}(\boldsymbol{z})$. According to the analysis in [43], [47], we set $\gamma = 1/\left(2 \max_k\{\|\mathbf{p}_k^{(n)}\|\}\right)$ to achieve the desired convergence rate. Besides, the use of Bregman distance $D(\boldsymbol{z}, \boldsymbol{z}_t)$ is to monitor the local geometry for improving the algorithm performance [50]. Specifically, Bregman distance $D(\boldsymbol{z}, \boldsymbol{z}_t)$ is induced by a mirror mapping function $\Phi(\boldsymbol{z}) : \mathbb{R}^{2N} \times \mathbb{R}^K \to \mathbb{R}$ for set $\mathcal{V} \times \mathcal{Y}$:

$$D(\boldsymbol{z}, \boldsymbol{z}_t) := \Phi(\boldsymbol{z}) - \Phi(\boldsymbol{z}_t) - \langle \nabla\Phi(\boldsymbol{z}_t), \boldsymbol{z} - \boldsymbol{z}_t \rangle. \quad (34)$$

We select the mapping function according to the structure of $\mathcal{V} \times \mathcal{Y}$ to attain the goal of capturing the local geometry. We choose $\Phi(\boldsymbol{z}) : \mathbb{R}^{2N} \times \mathbb{R}^K \to \mathbb{R}$ as

$$\Phi(\boldsymbol{z}) := \frac{1}{2}\|\tilde{\boldsymbol{v}}\|^2 + \sum_{k=1}^{K} y^k \log y^k,$$

where the first item and the second item are the mirror mapping functions for the Euclidean space (i.e., $\mathcal{V}$) and the simplex space (i.e., $\mathcal{Y}$), respectively. By substituting the expression of $\Phi(\boldsymbol{z})$ into (34), we have

$$D(\boldsymbol{z}, \boldsymbol{z}_t) = \frac{1}{2}\|\tilde{\boldsymbol{v}} - \tilde{\boldsymbol{v}}_t\|^2 + \sum_{k=1}^{K} y^k \log \frac{y^k}{y_t^k} - \sum_{k=1}^{K}(y^k - y_t^k), \quad (35)$$

where the first item is the Euclidean distance induced by the first item of $\Phi(\boldsymbol{z})$, and other two items are the Bregman distance in the simplex space induced by the second item of $\Phi(\boldsymbol{z})$.

Remark 3. The update of the Mirror-Prox method has an additional Step (33b) compared to the mirror descent method that only requires Step (33a). The computation of $\boldsymbol{z}_{t+1}'$ in (33a) is used to find a better direction $\mathbf{F}(\boldsymbol{z}_{t+1}')$ than the mirror descent method which is further used to update $\boldsymbol{z}_{t+1}$, i.e., (33b). This process is illustrated in Fig. 2. The Mirror-Prox method improves the convergence rate from $\mathcal{O}\left(\frac{1}{\sqrt{t}}\right)$ achieved by mirror descent to $\mathcal{O}\left(\frac{1}{t}\right)$ by using a more accurate update. We will show that the updates of (33a) and (33b) are of low complexity.

4) Implementation Details: At each iteration of the Mirror-Prox method, we need to efficiently solve Problems (33a) and (33b). Specifically, by introducing a variable $\boldsymbol{w}$, the update of $\boldsymbol{z}_{t+1}'$ in (33a) can be decomposed into the following three steps [43]

$$\nabla\Phi(\boldsymbol{w}) = \nabla\Phi(\boldsymbol{z}_t) - \gamma\mathbf{F}(\boldsymbol{z}_t), \quad (36a)$$

$$\boldsymbol{w} = \nabla\Phi^{-1}(\nabla\Phi(\boldsymbol{z}_t) - \gamma\mathbf{F}(\boldsymbol{z}_t)), \quad (36b)$$

$$\boldsymbol{z}_{t+1}' = \arg\min_{\boldsymbol{z}\in\mathcal{V}\times\mathcal{Y}}\{D(\boldsymbol{z}, \boldsymbol{w})\}. \quad (36c)$$

It is clear that (36a) is easy to compute. Furthermore, $\boldsymbol{w}$ in (36b) can be obtained in a closed form, since $\nabla\Phi(\cdot)$ and $\nabla\Phi^{-1}(\cdot)$ can analytically be expressed as

$$\nabla\Phi(\mathbf{z}) = \begin{bmatrix} \tilde{\boldsymbol{v}} \\ 1 + \log y_1 \\ \vdots \\ 1 + \log y_K \end{bmatrix}, \nabla\Phi^{-1}(\boldsymbol{\xi}) = \begin{bmatrix} \boldsymbol{\zeta} \\ \exp(\nu_1 - 1) \\ \exp(\nu_2 - 1) \\ \vdots \\ \exp(\nu_K - 1) \end{bmatrix},$$

where $\boldsymbol{\xi} = [\boldsymbol{\zeta}^\mathsf{T}, \boldsymbol{\nu}^\mathsf{T}]^\mathsf{T}$. Subsequently, we show that the solution of Problem (36c) also admits a closed form, which involves a projection problem on $\mathcal{V} \times \mathcal{Y}$. According to (35), we rewrite Problem (36c) as

$$\arg\min_{\boldsymbol{z}\in\mathcal{V}\times\mathcal{Y}}\{D(\boldsymbol{z}, \boldsymbol{w})\} = \arg\min_{\boldsymbol{z}\in\mathcal{V}\times\mathcal{Y}}\left\{\frac{1}{2}\|\tilde{\boldsymbol{v}} - \boldsymbol{u}\|^2 + \sum_{k=1}^{K} y^k \log \frac{y^k}{e^k} - \sum_{k=1}^{K}(y^k - e^k)\right\}, \quad (37)$$

where $\boldsymbol{w} = [\boldsymbol{u}^\mathsf{T}, \boldsymbol{e}^\mathsf{T}]^\mathsf{T}$. Problem (37) can be decomposed into two independent subproblems with respect to $\tilde{\boldsymbol{v}}$ and $\boldsymbol{y}$, respectively, given by

$$\tilde{\boldsymbol{v}}_{t+1}' = \arg\min_{\tilde{\boldsymbol{v}}\in\mathcal{V}}\left\{\frac{1}{2}\|\tilde{\boldsymbol{v}} - \boldsymbol{u}\|^2\right\}, \quad (38a)$$

$$\boldsymbol{y}_{t+1}' = \arg\min_{\boldsymbol{y}\in\mathcal{Y}}\left\{\sum_{k=1}^{K} y^k \log \frac{y^k}{e^k} - \sum_{k=1}^{K}(y^k - e^k)\right\}. \quad (38b)$$

Problem (38a) can be considered as a projection problem in the Euclidean space [48]. Therefore, $(\tilde{v}_{t+1}')_i, \ \forall \ i$, admit the following expression

$$(\tilde{v}_{t+1}')_i = \begin{cases} \frac{u_i}{\left(u_i^2 + u_{N+i}^2\right)^{\frac{1}{2}}}, & u_i^2 + u_{N+i}^2 \geq 1, \\ u_i, & \text{otherwise.} \end{cases} \quad (39)$$

Lemma 3. Problem (38b) is a projection problem in the simplex space. The optimal solution is given by

$$\boldsymbol{y}^* = \frac{\boldsymbol{e}}{\|\boldsymbol{e}\|_1}. \quad (40)$$

Proof. Please refer to Appendix E. $\square$

The above derivation for Problem (33a) can be directly applied to Problem (33b). The details of the proposed Mirror-Prox algorithm for solving Problem (32) is summarized in Algorithm 2.

B. Mirror-Prox Method for Non-smooth Convex Problem (26)

The method proposed for solving Problem (20) can be readily applied to solve Problem (26). We next sketch the process of transforming Problem (26) to its equivalent variational inequality problem. According to Lemma 1, Problem (26) is equivalent to the following problem

$$\min_{\tilde{\boldsymbol{m}}} \max_{\boldsymbol{y}} \left(\bar{\mathbf{P}}^{(n)}\tilde{\boldsymbol{m}} + \bar{\mathbf{q}}^{(n)}\right)^\mathsf{T} \boldsymbol{y} \quad (41)$$
$$\text{s.t.} \ \tilde{\boldsymbol{m}} \in \mathcal{M}, \ \boldsymbol{y} \in \mathcal{Y},$$

Algorithm 2: Mirror-Prox method for Problem (20)

Input: Initial point $\boldsymbol{z}_0 = \left[\tilde{\boldsymbol{v}}_0^{\mathsf{T}}, \boldsymbol{y}_0^{\mathsf{T}}\right]^{\mathsf{T}}$, threshold ϵ, and
stepsize $\gamma = \frac{1}{2 \max_k\{\|\mathbf{p}_k^{(n)}\|\}}$;

1 **for** $t = 1, 2, \ldots,$ **do**

2    $\mathbf{F}(\boldsymbol{z}_t) = \left[\left((\mathbf{P}^{(n)})^{\mathsf{T}}\boldsymbol{y}_t\right)^{\mathsf{T}}, -\left(\mathbf{P}^{(n)}\tilde{\boldsymbol{v}}_t + \mathbf{q}^{(n)}\right)^{\mathsf{T}}\right]^{\mathsf{T}}$;

3    $\nabla\Phi(\boldsymbol{w}) = \nabla\Phi(\boldsymbol{z}_t) - \gamma\mathbf{F}(\boldsymbol{z}_t)$;

4    $\boldsymbol{w} = \nabla\Phi^{-1}(\nabla\Phi(\boldsymbol{z}_t) - \gamma\mathbf{F}(\boldsymbol{z}_t))$;

5    $\boldsymbol{z}'_{t+1} = \underset{\boldsymbol{z}\in\mathcal{V}\times\mathcal{Y}}{\arg\min}\{D(\boldsymbol{z}, \boldsymbol{w})\}$;

6    $\nabla\Phi(\boldsymbol{w}) = \nabla\Phi(\boldsymbol{z}_t) - \gamma\mathbf{F}\left(\boldsymbol{z}'_{t+1}\right)$;

7    $\boldsymbol{w} = \nabla\Phi^{-1}(\nabla\Phi(\boldsymbol{z}_t) - \gamma\mathbf{F}\left(\boldsymbol{z}'_{t+1}\right))$;

8    $\boldsymbol{z}_{t+1} = \underset{\boldsymbol{z}\in\mathcal{V}\times\mathcal{Y}}{\arg\min}\{D(\boldsymbol{z}, \boldsymbol{w})\}$;

9   **If** $D(\boldsymbol{z}_t, \boldsymbol{z}_{t+1})$ less than ϵ, set $\boldsymbol{z}_* = \frac{1}{T}\sum_{t=1}^{T}\boldsymbol{z}_t$,
   break; **else go to Step 1**;

10 **end**

---

where $\bar{\mathbf{P}}^{(n)} = \left[\bar{\mathbf{p}}_1^{(n)}, \ldots, \bar{\mathbf{p}}_K^{(n)}\right]^{\mathsf{T}}$, $\bar{\mathbf{q}}^{(n)} = \left[\bar{q}_1^{(n)}, \ldots, \bar{q}_K^{(n)}\right]^{\mathsf{T}}$. By further denoting $\bar{\boldsymbol{z}} = \left[\tilde{\boldsymbol{m}}^{\mathsf{T}}, \boldsymbol{y}^{\mathsf{T}}\right]^{\mathsf{T}}$, $\varphi^{(n)}(\tilde{\boldsymbol{m}}, \boldsymbol{y}) = \left(\bar{\mathbf{P}}^{(n)}\tilde{\boldsymbol{m}} + \bar{\mathbf{q}}^{(n)}\right)^{\mathsf{T}}\boldsymbol{y}$, and

$$\bar{\mathbf{F}}(\bar{\boldsymbol{z}}) := \begin{bmatrix} \nabla_{\tilde{\boldsymbol{m}}}\varphi^{(n)}(\tilde{\boldsymbol{m}}, \boldsymbol{y}) \\ -\nabla_{\boldsymbol{y}}\varphi^{(n)}(\tilde{\boldsymbol{m}}, \boldsymbol{y}) \end{bmatrix} = \begin{bmatrix} (\bar{\mathbf{P}}^{(n)})^{\mathsf{T}}\boldsymbol{y} \\ -\left(\bar{\mathbf{P}}^{(n)}\tilde{\boldsymbol{m}} + \bar{\mathbf{q}}^{(n)}\right) \end{bmatrix}.$$

We denote the Lipschitz parameter of operator $\bar{\mathbf{F}}(\bar{\boldsymbol{z}})$ as $\bar{L}$. According to Lemma 2, we have $\bar{L} = \max_k\{\|\bar{\mathbf{p}}_k^{(n)}\|\}$. Problem (41) can be further transformed to the following variational inequality problem

$$\begin{aligned} \text{find} \quad & \bar{\boldsymbol{z}}^* \\ \text{s.t.} \quad & \bar{\mathbf{F}}\left(\bar{\boldsymbol{z}}^*\right)^{\mathsf{T}}\left(\bar{\boldsymbol{z}} - \bar{\boldsymbol{z}}^*\right) \geq 0, \forall\, \bar{\boldsymbol{z}} \in \mathcal{M}\times\mathcal{Y}, \quad (42) \\ & \bar{\boldsymbol{z}}^* \in \mathcal{M}\times\mathcal{Y}. \end{aligned}$$

Algorithm 2 can be applied to solve Problem (42) by replacing $\boldsymbol{z}$, $\mathbf{p}_k^{(n)}$, and $\mathbf{F}(\boldsymbol{z}_t)$ by $\bar{\boldsymbol{z}}$, $\bar{\mathbf{p}}_k^{(n)}$, and $\bar{\mathbf{F}}(\bar{\boldsymbol{z}}_t)$, respectively.

C. Computational Complexity

At each iteration of Algorithm 2, the computation complexity is dominated by Step 2. In Step 2, we take a matrix-vector multiplication to update operator $\mathbf{F}(\cdot)$. For the optimization of phase-shift vector $\tilde{\boldsymbol{v}} \in \mathbb{R}^{2N}$, the computation cost of operator $\mathbf{F}(\cdot)$ in Step 2 is $\mathcal{O}(NK)$. Besides, according to [43], Algorithm 2 can obtain an ϵ-optimal solution within $\mathcal{O}\left(\frac{L\log(N)}{\epsilon}\right)$ iterations. As a result, the computation complexity of Algorithm 2 is $\mathcal{O}\left(\frac{NKL\log(N)}{\epsilon}\right)$. In a similar manner, we can conclude that the computation complexity is $\mathcal{O}\left(\frac{MK\bar{L}\log(M)}{\epsilon}\right)$ for updating $\tilde{\boldsymbol{m}}$. The specific time savings in our problem achieved by the proposed algorithm will be further demonstrated in the following section via simulations.

V. SIMULATION RESULTS

In this section, we present sample simulation results to illustrate the performance of the proposed algorithm for minimizing the MSE of the RIS-assisted AirComp systems.

A. Simulation Settings

We consider a three-dimensional (3D) coordinate system. The AP and the RIS are, respectively, located at $(0, 0, 20)$ meters and $(100, 0, 20)$ meters, while the IoT devices are uniformly located within a circular region centered at $(100, 20, 0)$ meters with radius 20 meters. The antennas at the AP and the passive reflecting elements at the RIS are arranged as a uniform linear array and a uniform planar array, respectively. In the simulations, we consider both large-scale fading and small-scale fading for all the channels. The distance-dependent large-scale fading is modeled as $T_0(d/d_0)^{-\alpha}$, where T_0 is the path loss at the reference distance $d_0 = 1$ meter, d denotes the distance between the transmitter and the receiver, and α is the path loss exponent. We consider Rayleigh fading for the direct channel. Besides, we consider Rician fading for the reflecting links with Rician factor β. For the RIS-AP link (i.e., $\boldsymbol{G}$), we have

$$\boldsymbol{G} = \sqrt{T_0(d_{\mathrm{RA}}/d_0)^{-\alpha_{\mathrm{RA}}}}\left(\sqrt{\frac{\beta}{1+\beta}}\boldsymbol{G}^{\mathrm{LoS}} + \sqrt{\frac{1}{1+\beta}}\boldsymbol{G}^{\mathrm{NLoS}}\right),$$

where $\boldsymbol{G}^{\mathrm{LoS}}$ and $\boldsymbol{G}^{\mathrm{NLoS}}$ denote the line-of-sight (LoS) and the non-line-of-sight (NLoS) components, respectively, d_{RA} is the distance between the RIS and the AP, and α_{RA} is the path loss exponent. The channel coefficient of the link between IoT device k and the RIS, i.e., $\boldsymbol{h}_{\mathrm{r},k} \forall\, k$, is generated in a similar manner as $\boldsymbol{G}$. We set the path loss exponents of the device-AP links, the device-RIS links, and the RIS-AP link as 3.8, 2.5, and 2.2, respectively. Unless specified otherwise, we set $\beta = 3$, $T_0 = -30$ dB, $P = 30$ dBm, $\sigma^2 = -90$ dBm, and $\epsilon = 10^{-5}$.

B. Performance Evaluation

We investigate the convergence performance of the proposed Mirror-Prox based AlterMin SCA algorithm in Fig. 3. It can be observed that the MSE of our proposed algorithm monotonically decreases over the iterations and converges in a few iterations. In addition, the achieved MSE values of the proposed algorithms before and after the projection of the phase-shift vector at the RIS are almost the same. This is because, in the simulations, the obtained phase-shift vector always meets the constraints $|v_i| = 1, \forall\, i$ before projection.

We compare the proposed algorithm with the following four baseline methods.

- **Alternating SDR**: This method leverages the SDR technique [22], [38] to optimize $\boldsymbol{m}$ and $\boldsymbol{v}$ alternately. The Gaussian randomization technique is applied when the solution returned by the relaxed SDP problem does not meet the rank-one constraint. The number of randomization is set to be 50.
- **Alternating DC**: This method was proposed in [1], which reformulates the rank-one constrained SDP problem as a DC programming problem, followed by using SCA to obtain the rank-one solution via successively solving the convex approximation of the DC problem. Our comparison with this algorithm is only conducted when the number of IoT devices is small, i.e., low-density scenario, due to its high computational complexity.
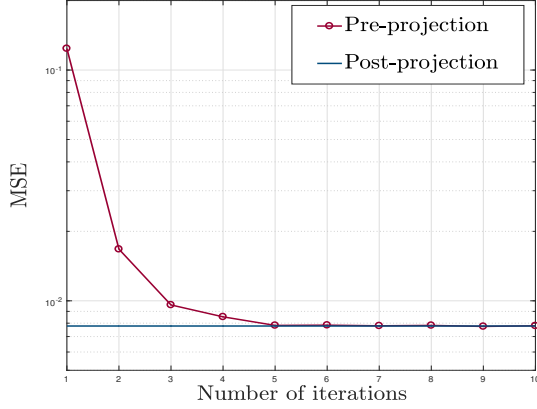
Fig. 3: Convergence behavior of the proposed algorithm when $N = 50$, $M = 10$, and $K = 200$.
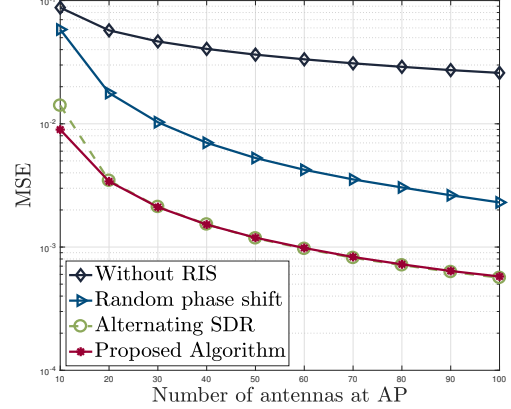

Fig. 4: MSE versus the number of antennas at AP when $K = 200$ and $N = 50$.

Fig. 5: Computation time versus the number of antennas at AP when $K = 200$ and $N = 50$.

- **Random phase shift**: With this method, the phase-shift matrix $\boldsymbol{\Theta}$ is randomly chosen and kept fixed when optimizing the receive beamforming vector $\boldsymbol{m}$ via our proposed algorithm.
- **Without RIS**: In the method, the signals are transmitted only through the direct links, i.e., $\boldsymbol{\Theta} = \boldsymbol{0}$. We only optimize the receive beamforming vector $\boldsymbol{m}$ via our proposed algorithm.

As the alternating SDR and alternating DC algorithms are not guaranteed to converge, we set their iteration numbers as the number of iterations required by our proposed algorithm to converge for a fair comparison. Based on the number of IoT devices in the network coverage area, we consider the high-density and low-density scenarios.

1) High-density Scenario: Fig. 4 shows the impact of the number of antennas at the AP (i.e., M) on the MSE when $N = 50$ and $K = 200$. As can be observed, for all methods under consideration, the MSE of the RIS-assisted AirComp system monotonically decreases as the number of antennas increases. This is because a greater diversity gain can be achieved by deploying a larger antenna array. We can also observe that deploying an RIS significantly reduces the MSE in the considered AirComp system. It shows that RIS is a promising technique that can enhance the performance of AirComp. Besides, we observe that the proposed algorithm outperforms the benchmark scheme with random phase-shift at the RIS, which reveals the necessity of optimizing the phase-shifts vector in RIS-assisted AirComp systems. Moreover, our proposed algorithm attains a similar performance as the alternating SDR algorithm. On the other hand, as can be observed in Fig. 5, our proposed algorithm significantly outperforms the alternating SDR algorithm in terms of the computation time. Besides, the advantage on the computation time of the proposed algorithm increases as the number of antennas at the AP becomes large. The reason is that the alternating SDR algorithm requires the execution of the second-order interior point method at each iteration, while the proposed algorithm as a first-order algorithm has a much lower computation complexity than the alternating SDR algorithm.

In Fig. 6, we investigate the impact of the number of the reflecting elements at the RIS on MSE when the number of IoT devices $K = 200$ and the number of antennas at the AP $M = 30$. As can be observed from Fig. 6, the proposed algorithm achieves almost the same MSE performance for different number of reflecting elements against the benchmark, which confirms the capability of our proposed algorithm to achieve high accurate AirComp. In addition, the MSE decreases significantly as the number of reflecting elements at the RIS increases. This is due to the fact that the RIS with more reflecting elements has more freedom for the reflection coefficient design. The computation time of our proposed algorithm and the alternating SDR algorithm versus the number of reflecting elements at the RIS is plotted in Fig. 7. As the number of reflecting elements at the RIS increases, the computation time of the alternating SDR algorithm increases significantly. Comparing with the alternating SDR algorithm, the proposed algorithm only consumes 1% and 26% of the computation time when $N = 100$ and $N = 30$, respectively.
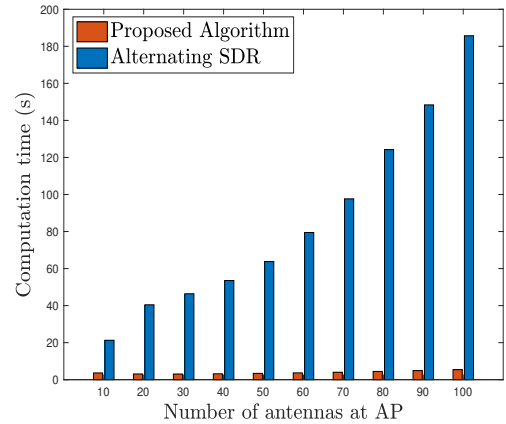
The computation time of the considered algorithms versus the number of IoT devices is illustratd in Fig. 8. It is obvious that, compared to the benchmark, our proposed algorithm has a superior performance in terms of the computation time. In particular, the reduction ratios are approximately 95% and 93% when $K = 300$ and $K = 100$, respectively. It can also
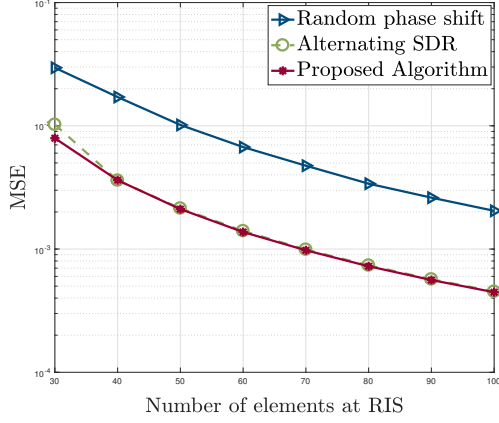
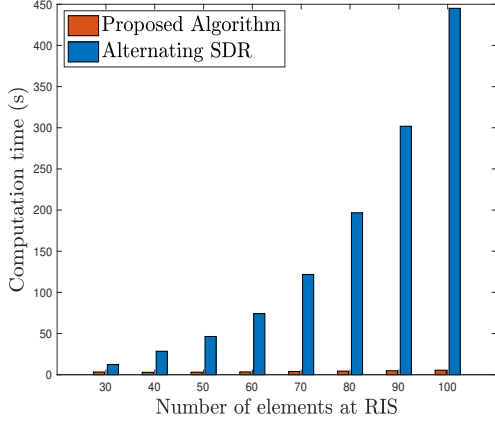Fig. 6: MSE versus the number of reflecting elements at RIS when $K = 200$ and $M = 30$.

Fig. 7: Computation time versus the number of reflecting elements at RIS when $K = 200$ and $M = 30$.

Fig. 8: Computation time versus the number of IoT devices when $M = 30$ and $N = 50$.

Fig. 9: MSE versus the number of antennas at AP when $K = 10$.

be observed that the superiority of the proposed algorithm in terms of the computation time enlarges as the number of IoT devices increases. This indicates the potentials of our proposed algorithm in high-density RIS-assisted AirComp systems.

TABLE I: Computation time (s) versus the number of antennas at AP when $K = 10$, $N = 40$.

Number of antennas at AP	5	10	15	20	25
Proposed Algorithm	0.5366	0.5541	0.5919	0.6635	0.8654
Alternating SDR	5.2860	6.7383	8.4276	9.7122	10.2587
Alternating DC	95.6772	96.5918	98.4988	101.1444	106.1467

2) Low-density Scenario: Due to the high computational complexity of the alternating DC algorithm, we compare its performance with the proposed algorithm when $K = 10$ in terms of the MSE and the computation time in Fig. 9 and TABLE I, respectively. It can be observed from Fig. 9 that the proposed algorithm achieves a lower MSE than the alternating SDR algorithm and attains a slightly higher MSE than the alternating DC algorithm. Besides, the MSE performance of all algorithms decreases as the number of reflecting elements at the RIS increases from 20 to 40. However, as shown in TABLE I, our proposed algorithm is remarkably better than the alternating SDR algorithm and the alternating DC algorithm in terms of the computation time.
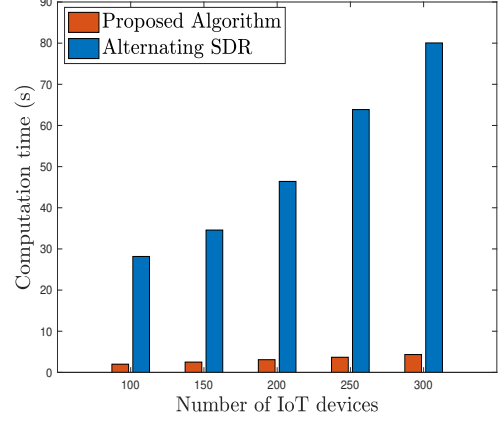
VI. CONCLUSION

In this paper, we proposed to leverage the advantage of RIS to mitigate the performance bottleneck of AirComp, thereby, achieving fast wireless data aggregation in IoT networks. We formulated an MSE minimization problem that requires the joint optimization of the transmit scalars at the IoT devices, the receive beamforming vector and the denoising factor at the AP, and the phase-shift matrix at the RIS. To solve this problem, a novel alternating minimization method in conjunction with the SCA technique was thus developed with convergence guarantee. To further reduce the computational complexity, we proposed a Mirror-Prox method that only involves a series of closed-form updates to solve the convex but non-smooth subproblem in each SCA iteration. Simulations showed that, compared to the existing alternating SDR and alternating DC algorithms, the proposed algorithm can significantly reduce the computation time while achieving a similar MSE performance.

APPENDIX

A. Proof of Proposition 1

For simplicity of notations, we denote

$$F_k(\boldsymbol{m}, \boldsymbol{v}) = \frac{\|\boldsymbol{m}\|^2}{|\boldsymbol{m}^{\mathsf{H}}(\boldsymbol{h}_{\mathrm{d},k} + \boldsymbol{G}\mathrm{diag}(\boldsymbol{h}_{\mathrm{r},k})\boldsymbol{v})|^2}, \ \forall \ k,$$

such that Problem (10) can be rewritten as

$$\min_{\boldsymbol{m},\boldsymbol{v}} \ \max_k F_k(\boldsymbol{m},\boldsymbol{v}) \tag{43}$$
$$\text{s.t.} \ |v_i| = 1, \forall \ i.$$

We then reformulate the problem into the following equivalent problem:

$$
\begin{array}{ll}
\min_{\boldsymbol{m},\boldsymbol{v}} \ \max_k F_k(\boldsymbol{m},\boldsymbol{v}) \\
\text{s.t.} \ |v_i| = 1, \forall \ i,
\end{array}
\iff
\begin{array}{ll}
\max_{\boldsymbol{m},\boldsymbol{v}} \ \left(\max_k F_k(\boldsymbol{m},\boldsymbol{v}) \right)^{-1} \\
\text{s.t.} \ |v_i| = 1, \forall \ i,
\end{array}
$$

$$
\iff
\begin{array}{ll}
\max_{\boldsymbol{m},\boldsymbol{v}} \ \min_k F_k^{-1}(\boldsymbol{m},\boldsymbol{v}) \\
\text{s.t.} \ |v_i| = 1, \forall \ i,
\end{array}
$$

where $F_k^{-1}(\boldsymbol{m},\boldsymbol{v}) = \frac{1}{F_k(\boldsymbol{m},\boldsymbol{v})}$. As a result, Problem (10) is equivalent to

$$\max_{\boldsymbol{m},\boldsymbol{v}} \ \left\{ \min_k \frac{|\boldsymbol{m}^{\mathsf{H}}(\boldsymbol{h}_{\mathrm{d},k} + \boldsymbol{G}\mathrm{diag}(\boldsymbol{h}_{\mathrm{r},k})\boldsymbol{v})|^2}{\|\boldsymbol{m}\|^2} \right\} \tag{44}$$
$$\text{s.t.} \ |v_n| = 1, \forall \ n = 1, \ldots, N.$$

Besides, we introduce an auxiliary variable $\tau = \|\boldsymbol{m}\|^2$. Problem (44) can be rewritten as the following form

$$\max_{\boldsymbol{m},\boldsymbol{v},\tau} \ \left\{ \min_k \frac{|\boldsymbol{m}^{\mathsf{H}}(\boldsymbol{h}_{\mathrm{d},k} + \boldsymbol{G}\mathrm{diag}(\boldsymbol{h}_{\mathrm{r},k})\boldsymbol{v})|^2}{\tau} \right\} \tag{45}$$
$$\text{s.t.} \ |v_n| = 1, \forall \ n = 1, \ldots, N,$$
$$\|\boldsymbol{m}\|^2 = \tau.$$

By denoting $\hat{\boldsymbol{m}} = \frac{\boldsymbol{m}}{\sqrt{\tau}}$, Problem (45) can be represented as

$$\max_{\hat{\boldsymbol{m}},\boldsymbol{v}} \ \left\{ \min_k |\hat{\boldsymbol{m}}^{\mathsf{H}}(\boldsymbol{h}_{\mathrm{d},k} + \boldsymbol{G}\mathrm{diag}(\boldsymbol{h}_{\mathrm{r},k})\boldsymbol{v})|^2 \right\} \tag{46}$$
$$\text{s.t.} \ |v_n| = 1, \forall \ n = 1, \ldots, N,$$
$$\|\hat{\boldsymbol{m}}\|^2 = 1.$$

We further transform Problem (46) to its equivalent problem in the min-max form as follows

$$
\begin{array}{ll}
\max_{\hat{\boldsymbol{m}},\boldsymbol{v}} \ \left\{ \min_k |\hat{\boldsymbol{m}}^{\mathsf{H}}(\boldsymbol{h}_{\mathrm{d},k} + \boldsymbol{G}\mathrm{diag}(\boldsymbol{h}_{\mathrm{r},k})\boldsymbol{v})|^2 \right\} \\
\text{s.t.} \ |v_n| = 1, \forall \ n = 1, \ldots, N, \\
\|\hat{\boldsymbol{m}}\|^2 = 1.
\end{array}
$$

$$
\iff
\begin{array}{ll}
\min_{\hat{\boldsymbol{m}},\boldsymbol{v}} \ \left\{ -\min_k |\hat{\boldsymbol{m}}^{\mathsf{H}}(\boldsymbol{h}_{\mathrm{d},k} + \boldsymbol{G}\mathrm{diag}(\boldsymbol{h}_{\mathrm{r},k})\boldsymbol{v})|^2 \right\} \\
\text{s.t.} \ |v_n| = 1, \forall \ n = 1, \ldots, N, \\
\|\hat{\boldsymbol{m}}\|^2 = 1.
\end{array}
$$

$$
\iff
\begin{array}{ll}
\min_{\hat{\boldsymbol{m}},\boldsymbol{v}} \ \max_k \left\{ -|\hat{\boldsymbol{m}}^{\mathsf{H}}(\boldsymbol{h}_{\mathrm{d},k} + \boldsymbol{G}\mathrm{diag}(\boldsymbol{h}_{\mathrm{r},k})\boldsymbol{v})|^2 \right\} \\
\text{s.t.} \ |v_n| = 1, \forall \ n = 1, \ldots, N, \\
\|\hat{\boldsymbol{m}}\|^2 = 1.
\end{array}
$$

To this end, we complete the proof.

B. Proof of Proposition 2

We first prove property (i). Considering the l-th alternating iteration, for a given $\tilde{m}_{(l)}^{(0)}$, we denote the objective value of Problem (18) as $f_{(l)}^v(\tilde{\boldsymbol{v}})$. We consider the SCA iteration that

starts from $\tilde{\boldsymbol{v}}_{(l)}^{(0)}$. By denoting $\hat{f}_{(l)}^v(\tilde{\boldsymbol{v}}, \tilde{\boldsymbol{v}}_{(l)}^{(n)})$ as the objective value of Problem (20), it satisfies
1) $\hat{f}_{(l)}^v(\tilde{\boldsymbol{v}}_{(l)}^{(n)}, \tilde{\boldsymbol{v}}_{(l)}^{(n)}) = f_{(l)}^v(\tilde{\boldsymbol{v}}_{(l)}^{(n)})$,
2) $f_{(l)}^v(\tilde{\boldsymbol{v}}_{(l)}^{(n+1)}) \le \hat{f}_{(l)}^v(\tilde{\boldsymbol{v}}_{(l)}^{(n+1)}, \tilde{\boldsymbol{v}}_{(l)}^{(n)})$,
3) $\hat{f}_{(l)}^v(\tilde{\boldsymbol{v}}_{(l)}^{(n+1)}, \tilde{\boldsymbol{v}}_{(l)}^{(n)}) \le \hat{f}_{(l)}^v(\tilde{\boldsymbol{v}}_{(l)}^{(n)}, \tilde{\boldsymbol{v}}_{(l)}^{(n)})$.

Inequality 1) holds since $\hat{f}_{(l)}^v(\tilde{\boldsymbol{v}}, \tilde{\boldsymbol{v}}_{(l)}^{(n)})$ is a linear approximation of $f_{(l)}^v(\tilde{\boldsymbol{v}})$ at point $\tilde{\boldsymbol{v}}_{(l)}^{(n)}$. According to (19), $\hat{f}_{(l)}^v(\tilde{\boldsymbol{v}}, \tilde{\boldsymbol{v}}_{(l)}^{(n)})$ is an upper bound of $f_{(l)}^v(\tilde{\boldsymbol{v}})$. As a result, we can establish inequality 2). Besides, inequality 3) holds as $\tilde{\boldsymbol{v}}_{(l)}^{(n+1)} = \arg\min_{\tilde{\boldsymbol{v}} \in \mathcal{V}} \hat{f}_{(l)}^v(\tilde{\boldsymbol{v}}, \tilde{\boldsymbol{v}}_{(l)}^{(n)})$. Hence, we obtain the following chain inequalities

$$f_{(l)}^v(\tilde{\boldsymbol{v}}_{(l)}^{(n+1)}) \le \hat{f}_{(l)}^v(\tilde{\boldsymbol{v}}_{(l)}^{(n+1)}, \tilde{\boldsymbol{v}}_{(l)}^{(n)}) \le \hat{f}_{(l)}^v(\tilde{\boldsymbol{v}}_{(l)}^{(n)}, \tilde{\boldsymbol{v}}_{(l)}^{(n)}) = f_{(l)}^v(\tilde{\boldsymbol{v}}_{(l)}^{(n)}).$$

Besides, the continuous function $f_{(l)}^v(\tilde{\boldsymbol{v}})$ has a lower bound in the constrained set. As a result, the non-increasing and lower bounded sequence $\{f_{(l)}^v(\tilde{\boldsymbol{v}}_{(l)}^{(n)})\}$ converges. Similarly, we can establish the non-increasing and convergent property for the objective value sequence achieved by $\{\tilde{m}_{(l)}^{(n)}\}_{n=0}^{\infty}$. To this end, we have proved property i).

On the other hand, we can prove property ii) by iteratively utilizing property i).

C. Proof of Lemma 1

We have shown that Problem (20) is equivalent to Problem (27). We then rewrite Problem (27) in a more compact form as

$$\min_{\tilde{\boldsymbol{v}},r} \ r$$
$$\text{s.t.} \ \mathbf{P}^{(n)}\tilde{\boldsymbol{v}} + \mathbf{q}^{(n)} - r\mathbf{1} \preceq 0, \tag{47}$$
$$\tilde{\boldsymbol{v}} \in \mathcal{V}, \ r \in \mathbb{R}.$$

where $\mathbf{1} = [1,1,\ldots,1]^{\mathsf{T}} \in \mathbb{R}^K$. For a given vector $\boldsymbol{y} \in \mathbb{R}^K$ with non-negative components, which is known as dual variable, the corresponding Lagrangian relaxed problem is given by

$$\min_{\tilde{\boldsymbol{v}},r} \ r + \boldsymbol{y}^{\mathsf{T}}\left(\mathbf{P}^{(n)}\tilde{\boldsymbol{v}} + \mathbf{q}^{(n)} - r\mathbf{1}\right)$$
$$\text{s.t.} \ \tilde{\boldsymbol{v}} \in \mathcal{V}, \ r \in \mathbb{R}. \tag{48}$$

We reorganize the objective function of Problem (48) as

$$\left(1 - \mathbf{1}^{\mathsf{T}}\boldsymbol{y}\right)r + \left(\mathbf{P}^{(n)}\tilde{\boldsymbol{v}} + \mathbf{q}^{(n)}\right)^{\mathsf{T}}\boldsymbol{y}.$$

The dual objective function of Problem (47) is given by the optimal value of Problem (48). If $1 - \mathbf{1}^{\mathsf{T}}\boldsymbol{y} \neq 0$, then $\left(1 - \mathbf{1}^{\mathsf{T}}\boldsymbol{y}\right)r$ is not bounded from below, since $\left(1 - \mathbf{1}^{\mathsf{T}}\boldsymbol{y}\right)r \to -\infty$ if $\mathbf{1}^{\mathsf{T}}\boldsymbol{y} > 1$ and $r \to +\infty$ or if $\mathbf{1}^{\mathsf{T}}\boldsymbol{y} < 1$ and $r \to -\infty$.

Thus, we only need to consider $\boldsymbol{y} \in \mathbb{R}^K$ that satisfy $\boldsymbol{y} \geq \mathbf{0}$ and $\mathbf{1}^{\mathsf{T}}\boldsymbol{y} = 1$. For these $\boldsymbol{y}$, the dual objective function is given by $\min_{\tilde{\boldsymbol{v}} \in \mathcal{V}}\left(\mathbf{P}^{(n)}\tilde{\boldsymbol{v}} + \mathbf{q}^{(n)}\right)^{\mathsf{T}}\boldsymbol{y}$. The dual problem is

$$\max_{\boldsymbol{y}} \ \min_{\tilde{\boldsymbol{v}}} \ \left(\mathbf{P}^{(n)}\tilde{\boldsymbol{v}} + \mathbf{q}^{(n)}\right)^{\mathsf{T}}\boldsymbol{y}$$
$$\text{s.t.} \ \tilde{\boldsymbol{v}} \in \mathcal{V}, \ \boldsymbol{y} \in \mathcal{Y}. \tag{49}$$

Because the original problem is convex and set $\mathcal{V}$ is closed and compact, the strong duality condition is satisfied. Hence, its

dual problem is equivalent to itself. As the objective function $\left(\mathbf{P}^{(n)}\tilde{\boldsymbol{v}} + \mathbf{q}^{(n)}\right)^\mathsf{T} \boldsymbol{y}$ is linear to $\tilde{\boldsymbol{v}}$ and $\boldsymbol{y}$, according to [48], Problem (49) is equivalent to Problem (28), which is a smooth convex-concave saddle point problem [47].

D. Proof of Lemma 2

$\mathbf{F}(\cdot)$ is a linear operator with well-defined monotonicity. According to [43], the definition of the L-Lipschitz property of operator $\mathbf{F}(\boldsymbol{z})$ enforces the following constraints

a). $\left\|\nabla_{\tilde{\boldsymbol{v}}}\psi^{(n)}(\tilde{\boldsymbol{v}}, \boldsymbol{y}) - \nabla_{\tilde{\boldsymbol{v}}}\psi^{(n)}\left(\tilde{\boldsymbol{v}}', \boldsymbol{y}\right)\right\|_{\mathcal{V}}^* \leq L \cdot \|\tilde{\boldsymbol{v}} - \tilde{\boldsymbol{v}}'\|_{\mathcal{V}}$,

b). $\left\|\nabla_{\tilde{\boldsymbol{v}}}\psi^{(n)}(\tilde{\boldsymbol{v}}, \boldsymbol{y}) - \nabla_{\tilde{\boldsymbol{v}}}\psi^{(n)}\left(\tilde{\boldsymbol{v}}, \boldsymbol{y}'\right)\right\|_{\mathcal{Y}}^* \leq L \cdot \|\boldsymbol{y} - \boldsymbol{y}'\|_{\mathcal{Y}}$,

c). $\left\|\nabla_{\boldsymbol{y}}\psi^{(n)}(\tilde{\boldsymbol{v}}, \boldsymbol{y}) - \nabla_{\boldsymbol{y}}\psi^{(n)}\left(\tilde{\boldsymbol{v}}, \boldsymbol{y}'\right)\right\|_{\mathcal{Y}}^* \leq L \cdot \|\boldsymbol{y} - \boldsymbol{y}'\|_{\mathcal{Y}}$,

d). $\left\|\nabla_{\boldsymbol{y}}\psi^{(n)}(\tilde{\boldsymbol{v}}, \boldsymbol{y}) - \nabla_{\boldsymbol{y}}\psi^{(n)}\left(\tilde{\boldsymbol{v}}', \boldsymbol{y}\right)\right\|_{\mathcal{Y}}^* \leq L \cdot \|\tilde{\boldsymbol{v}} - \tilde{\boldsymbol{v}}'\|_{\mathcal{V}}$,

where $\|\cdot\|_{\mathcal{V}}$ and $\|\cdot\|_{\mathcal{Y}}$ denote the norms embedded in spaces $\mathcal{V}$ and $\mathcal{Y}$ respectively, and $\|\cdot\|_{\mathcal{V}}^*$ and $\|\cdot\|_{\mathcal{Y}}^*$ denote the dual norms of $\|\cdot\|_{\mathcal{V}}$ and $\|\cdot\|_{\mathcal{Y}}$, respectively. To show the L-Lipschitz property of $\mathbf{F}(\cdot)$, we need to verify the above inequalities. In our work, $\|\cdot\|_{\mathcal{V}}$ and $\|\cdot\|_{\mathcal{Y}}$ are defined as ℓ_2 and ℓ_1 norms, respectively. As a result, $\|\cdot\|_{\mathcal{V}}^*$ and $\|\cdot\|_{\mathcal{Y}}^*$ represent ℓ_2 and ℓ_∞ norms, respectively. First, inequalities a) and c) hold due to the fact that

$$\nabla_{\tilde{\boldsymbol{v}}}\psi^{(n)}(\tilde{\boldsymbol{v}}, \boldsymbol{y}) = \nabla_{\tilde{\boldsymbol{v}}}, \psi^{(n)}\left(\tilde{\boldsymbol{v}}', \boldsymbol{y}\right) = (\mathbf{P}^{(n)})^\mathsf{T}\boldsymbol{y},$$
$$\nabla_{\boldsymbol{y}}\psi^{(n)}(\tilde{\boldsymbol{v}}, \boldsymbol{y}) = \nabla_{\boldsymbol{y}}\psi^{(n)}\left(\tilde{\boldsymbol{v}}, \boldsymbol{y}'\right) = \mathbf{P}^{(n)}\tilde{\boldsymbol{v}} + \mathbf{q}^{(n)}.$$

Inequality b) holds since

$$\left\|\nabla_{\tilde{\boldsymbol{v}}}\psi^{(n)}(\tilde{\boldsymbol{v}}, \boldsymbol{y}) - \nabla_{\tilde{\boldsymbol{v}}}\psi^{(n)}\left(\tilde{\boldsymbol{v}}, \boldsymbol{y}'\right)\right\|$$

$$= \|(\mathbf{P}^{(n)})^\mathsf{T}\boldsymbol{y} - (\mathbf{P}^{(n)})^\mathsf{T}\boldsymbol{y}'\| = \|\sum_{k=1}^{K}\mathbf{p}_k^{(n)}(y_k - y_k')\|$$

$$\leq \sum_{k=1}^{K}\|\mathbf{p}_k^{(n)}\| \cdot |y_k - y_k'| \leq \left(\max_k\|\mathbf{p}_k^{(n)}\|\right) \cdot \left(\sum_{k=1}^{K}|y_k - y_k'|\right)$$

$$= L \cdot \|\boldsymbol{y} - \boldsymbol{y}'\|_1.$$

Finally, inequality d) holds as

$$\left\|\nabla_{\boldsymbol{y}}\psi^{(n)}(\tilde{\boldsymbol{v}}, \boldsymbol{y}) - \nabla_{\boldsymbol{y}}\psi^{(n)}\left(\tilde{\boldsymbol{v}}', \boldsymbol{y}'\right)\right\|_\infty = \|\mathbf{P}^{(n)}\tilde{\boldsymbol{v}} - \mathbf{P}^{(n)}\tilde{\boldsymbol{v}}'\|_\infty$$

$$= \max_k\left\{\left|\left(\mathbf{p}_k^{(n)}\right)^\mathsf{T}(\tilde{\boldsymbol{v}} - \tilde{\boldsymbol{v}}')\right|\right\}$$

$$\underset{(a)}{\leq} \left(\max_k\|\mathbf{p}_k^{(n)}\|\right) \cdot \|\tilde{\boldsymbol{v}} - \tilde{\boldsymbol{v}}'\| = L \cdot \|\tilde{\boldsymbol{v}} - \tilde{\boldsymbol{v}}'\|,$$

where (a) follows by applying the Cauchy-Schwarz inequality.

E. Proof of Lemma 3

We rewrite Problem (38b) as

$$\min_{\boldsymbol{y}} \left\{\sum_{k=1}^{K} y^k \log \frac{y^k}{e^k} - \sum_{k=1}^{K}\left(y^k - e^k\right)\right\} \tag{50}$$
$$\text{s.t. } \mathbf{1}^\mathsf{T}\boldsymbol{y} = 1.$$

By introducing a Lagrangian multiplier μ for the equality constraint, the Lagrangian function of Problem (50) can be expressed as

$$L(\boldsymbol{y}, \mu) = \sum_{k=1}^{K} y^k \log \frac{y^k}{e^k} - \sum_{k=1}^{K}\left(y^k - e^k\right) + \mu \cdot (\mathbf{1}^\mathsf{T}\boldsymbol{y} - 1).$$

According to the KKT condition, we have

$$1 + \log(y_k^*) - \log(e_k) - 1 + \mu = 0, \ \forall k. \tag{51}$$

Note that $e_k > 0$ according to (36b). One thus can claim that $y_k^* = e_k/\exp(\mu)$. Besides, we can conclude that $\exp(\mu) = \sum_{k=1}^{K} e_k$ as $\mathbf{1}^\mathsf{T}\boldsymbol{y}^* = 1$. Therefore, we have $\boldsymbol{y}^* = \boldsymbol{e}/\|\boldsymbol{e}\|_1$.

REFERENCES

[1] T. Jiang and Y. Shi, "Over-the-air computation via intelligent reflecting surfaces," in *Proc. IEEE Global Commun. Conf. (Globecom)*, Waikoloa, HI, Dec. 2019.

[2] K. W. Choi, A. A. Aziz, D. Setiawan, N. M. Tran, L. Ginting, and D. I. Kim, "Distributed wireless power transfer system for Internet of things devices," *IEEE Internet Things J.*, vol. 5, no. 4, pp. 2657–2671, Aug. 2018.

[3] C. Intanagonwiwat, R. Govindan, D. Estrin, J. Heidemann, and F. Silva, "Directed diffusion for wireless sensor networking," *IEEE/ACM Trans. Netw.*, vol. 11, no. 1, pp. 2–16, Feb. 2003.

[4] W. B. Heinzelman, A. P. Chandrakasan, and H. Balakrishnan, "An application-specific protocol architecture for wireless microsensor networks," *IEEE Trans. Wireless Commun.*, vol. 1, no. 4, pp. 660–670, Oct. 2002.

[5] B. Nazer and M. Gastpar, "Computation over multiple-access channels," *IEEE Trans. Inf. Theory*, vol. 53, no. 10, pp. 3498–3516, Oct. 2007.

[6] W. Liu, X. Zang, Y. Li, and B. Vucetic, "Over-the-air computation systems: Optimization, analysis and scaling laws," *IEEE Trans. Wireless Commun.*, vol. 19, no. 8, pp. 5488–5502, Aug. 2020.

[7] X. Cao, G. Zhu, J. Xu, and K. Huang, "Optimized power control for over-the-air computation in fading channels," *IEEE Trans. Wireless Commun.*, vol. 19, no. 11, pp. 7498–7513, Nov. 2020.

[8] L. Chen, X. Qin, and G. Wei, "A uniform-forcing transceiver design for over-the-air function computation," *IEEE Wireless Commun. Lett.*, vol. 7, no. 6, pp. 942–945, Dec. 2018.

[9] L. Chen, N. Zhao, Y. Chen, F. R. Yu, and G. Wei, "Over-the-air computation for IoT networks: Computing multiple functions with antenna arrays," *IEEE Internet Things J.*, vol. 5, no. 6, pp. 5296–5306, Jun. 2018.

[10] G. Zhu and K. Huang, "MIMO over-the-air computation for high-mobility multimodal sensing," *IEEE Internet Things J.*, vol. 6, no. 4, pp. 6089–6103, Aug. 2019.

[11] J. Dong, Y. Shi, and Z. Ding, "Blind over-the-air computation and data fusion via provable wirtinger flow," *IEEE Trans. Signal Process.*, vol. 68, pp. 1136–1151, Jan. 2020.

[12] L. Chen, N. Zhao, Y. Chen, F. R. Yu, and G. Wei, "Toward optimal rate-delay tradeoff for computation over multiple access channel," *IEEE Trans. Commun.*, Mar. 2021, doi: 10.1109/TCOMM.2021.3068493.

[13] F. Wu, L. Chen, N. Zhao, Y. Chen, F. R. Yu, and G. Wei, "Computation over multi-access channels: Multi-hop implementation and resource allocation," *IEEE Trans. Commun.*, vol. 69, no. 2, pp. 1038–1052, Feb. 2021.

[14] M. Frey, I. Bjelakovic, and S. Stanczak, "Over-the-air computation in correlated channels," 2021. [Online]. Available: https://arxiv.org/abs/2101.04690

[15] W. Liu, X. Zang, B. Vucetic, and Y. Li, "Over-the-air computation with spatial-and-temporal correlated signals," *IEEE Wireless Communications Letters*, vol. 10, no. 7, pp. 1591–1595, Jul. 2021.

[16] Y. Shao, D. Gunduz, and S. C. Liew, "Federated edge learning with misaligned over-the-air computation," *arXiv preprint arXiv:2102.13604*, 2021. [Online]. Available: https://arxiv.org/abs/2102.13604

[17] K. Yang, T. Jiang, Y. Shi, and Z. Ding, "Federated learning via over-the-air computation," *IEEE Trans. Wireless Commun.*, vol. 19, no. 3, pp. 2022–2035, Mar. 2020.

[18] M. Mohammadi Amiri and D. Gündüz, "Machine learning at the wireless edge: Distributed stochastic gradient descent over-the-air," *IEEE Trans. Signal Process.*, vol. 68, pp. 2155–2169, Mar. 2020.

[19] K. Yang, Y. Shi, Y. Zhou, Z. Yang, L. Fu, and W. Chen, "Federated machine learning for intelligent IoT via reconfigurable intelligent surface," *IEEE Netw.*, vol. 34, no. 5, pp. 16–22, Oct. 2020.

[20] C. Liaskos, S. Nie, A. Tsioliaridou, A. Pitsillides, S. Ioannidis, and I. Akyildiz, "A new wireless communication paradigm through software-controlled metasurfaces," *IEEE Commun. Mag.*, vol. 56, no. 9, pp. 162–169, Sept. 2018.

[21] Q. Wu and R. Zhang, "Towards smart and reconfigurable environment: Intelligent reflecting surface aided wireless network," *IEEE Commun. Mag.*, vol. 58, no. 1, pp. 106–112, Jan. 2020.

[22] Q. Wu and R. Zhang, "Intelligent reflecting surface enhanced wireless network via joint active and passive beamforming," *IEEE Trans. Wireless Commun.*, vol. 18, no. 11, pp. 5394–5409, Nov. 2019.

[23] C. Huang, A. Zappone, G. C. Alexandropoulos, M. Debbah, and C. Yuen, "Reconfigurable intelligent surfaces for energy efficiency in wireless communication," *IEEE Trans. Wireless Commun.*, vol. 18, no. 8, pp. 4157–4170, Aug. 2019.

[24] X. Yuan, Y. J. Angela Zhang, Y. Shi, W. Yan, and H. Liu, "Reconfigurable-intelligent-surface empowered wireless communications: Challenges and opportunities," *IEEE Wireless Commun.*, pp. 1–8, Feb. 2021, doi:10.1109/MWC.001.2000256.

[25] M. Fu, Y. Zhou, Y. Shi, and K. B. Letaief, "Reconfigurable intelligent surface empowered downlink non-orthogonal multiple access," *IEEE Trans. Commun.*, 2021, doi: 10.1109/TCOMM.2021.3066587.

[26] S. Xia, Y. Shi, Y. Zhou, and X. Yuan, "Reconfigurable intelligent surface for massive connectivity," 2021. [Online]. Available: https://arxiv.org/abs/2101.10322

[27] J. He, K. Yu, Y. Shi, Y. Zhou, W. Chen, and K. B. Letaief, "Reconfigurable intelligent surface assisted massive MIMO with antenna selection," 2020. [Online]. Available: https://arxiv.org/abs/2009.07546

[28] P. Wang, J. Fang, X. Yuan, Z. Chen, and H. Li, "Intelligent reflecting surface-assisted millimeter wave communications: Joint active and passive precoding design," *IEEE Trans. Veh. Technol.*, vol. 69, no. 12, pp. 14 960–14 973, Dec. 2020.

[29] S. Li, B. Duo, X. Yuan, Y. Liang, and M. Di Renzo, "Reconfigurable intelligent surface assisted UAV communication: Joint trajectory design and passive beamforming," *IEEE Wireless Commun. Lett.*, vol. 9, no. 5, pp. 716–720, May 2020.

[30] C. Pan, H. Ren, K. Wang, M. Elkashlan, A. Nallanathan, J. Wang, and L. Hanzo, "Intelligent reflecting surface aided MIMO broadcasting for simultaneous wireless information and power transfer," *IEEE J. Sel. Areas Commun.*, vol. 38, no. 8, pp. 1719–1734, Aug. 2020.

[31] Y. Yang, B. Zheng, S. Zhang, and R. Zhang, "Intelligent reflecting surface meets OFDM: Protocol design and rate maximization," *IEEE Trans. Commun.*, vol. 68, no. 7, pp. 4522–4535, Jul. 2020.

[32] H. Liu, X. Yuan, and Y. J. A. Zhang, "Matrix-calibration-based cascaded channel estimation for reconfigurable intelligent surface assisted multiuser MIMO," *IEEE J. Sel. Areas Commun.*, vol. 38, no. 11, pp. 2621–2636, Nov. 2020.

[33] Z. Wang, L. Liu, and S. Cui, "Channel estimation for intelligent reflecting surface assisted multiuser communications: Framework, algorithms, and analysis," *IEEE Trans. Wireless Commun.*, vol. 19, no. 10, pp. 6607–6620, Oct. 2020.

[34] X. Guan, Q. Wu, and R. Zhang, "Anchor-assisted channel estimation for intelligent reflecting surface aided multiuser communication," 2021. [Online]. Available: https://arxiv.org/abs/2102.10886

[35] G. Zhou, C. Pan, H. Ren, K. Wang, M. D. Renzo, and A. Nallanathan, "Robust beamforming design for intelligent reflecting surface aided MISO communication systems," *IEEE Wireless Commun. Lett.*, vol. 9, no. 10, pp. 1658–1662, Oct. 2020.

[36] W. Fang, M. Fu, K. Wang, Y. Shi, and Y. Zhou, "Stochastic beamforming for reconfigurable intelligent surface aided over-the-air computation," in *Proc. IEEE Global Commun. Conf. (Globecom)*, Dec. 2020.

[37] G. Zhou, C. Pan, H. Ren, K. Wang, and A. Nallanathan, "A framework of robust transmission design for IRS-aided MISO communications with imperfect cascaded channels," *IEEE Trans. Signal Process.*, vol. 68, pp. 5092–5106, Aug. 2020.

[38] Z. Wang, Y. Shi, Y. Zhou, H. Zhou, and N. Zhang, "Wireless-powered over-the-air computation in intelligent reflecting surface-aided IoT networks," *IEEE Internet Things J.*, vol. 8, no. 3, pp. 1585–1598, Feb. 2021.

[39] X. Li, G. Zhu, Y. Gong, and K. Huang, "Wirelessly powered data aggregation for IoT via over-the-air function computation: Beamforming and power control," *IEEE Trans. Wireless Commun.*, vol. 18, no. 7, pp. 3437–3452, Jul. 2019.

[40] X. Yu, D. Xu, D. W. K. Ng, and R. Schober, "Power-efficient resource allocation for multiuser MISO systems via intelligent reflecting surfaces," in *Proc. IEEE Global Commun. Conf. (Globecom)*, Taiwan, Dec. 2020.

[41] Y. Nesterov and A. Nemirovskii, *Interior-Point Polynomial Algorithms in Convex Programming*. Soc. Ind. Appl. Math., 1994.

[42] N. D. Sidiropoulos and T. N. Davidson, "Broadcasting with channel state information," in *Proc. IEEE Sensor Array Multichannel Signal Process. Workshop*, Jul. 2004, pp. 489–493.

[43] S. Bubeck, "Convex optimization: Algorithms and complexity," *Found. Trends Mach. Learn.*, vol. 8, no. 3-4, pp. 231–357, 2015.

[44] G. Zhou, C. Pan, H. Ren, K. Wang, and A. Nallanathan, "Intelligent reflecting surface aided multigroup multicast MISO communication systems," *IEEE Trans. Signal Process.*, vol. 68, pp. 3236–3251, Apr. 2020.

[45] Z. Peng, Z. Zhang, C. Pan, L. Li, and A. L. Swindlehurst, "Multiuser full-duplex two-way communications via intelligent reflecting surface," *IEEE Trans. Signal Process.*, vol. 69, pp. 837–851, Jan. 2021.

[46] A. Beck, *First-order methods in optimization*. Philadelphia, PA, USA: SIAM, 2017.

[47] A. Nemirovski, "Prox-method with rate of convergence o(1/t) for variational inequalities with lipschitz continuous monotone operators and smooth convex-concave saddle point problems," *SIAM J. Optim.*, vol. 15, no. 1, pp. 229–251, 2004.

[48] S. Boyd and L. Vandenberghe, *Convex Optimization*. Cambridge Univ. Press, 2004.

[49] E. K. Ryu and S. Boyd, "Primer on monotone operator methods," *Appl. Comput. Math*, vol. 15, no. 1, pp. 3–43, 2016.

[50] A. Nemirovskii, D. Yudin, and Wiley, "Problem complexity and method efficiency in optimization," 1983.

[51] M. S. Ibrahim, A. Konar, M. Hong, and N. D. Sidiropoulos, "Mirror-prox SCA algorithm for multicast beamforming and antenna selection," in *Proc. IEEE SPAWC*, Kalamata, Greece, Jun. 2018.

Wenzhi Fang (Student Member, IEEE) received the B.S. degree from the School of Communication & Information Engineering, Shanghai University, Shanghai, China, in 2020. He is currently pursing a master degree with the School of Information Science and Technology, ShanghaiTech University, Shanghai, China. His research areas include optimization, machine learning, wireless communications, and their applications to 6G, IoT, and AI.
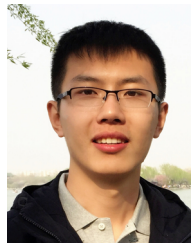
Yuning Jiang (Member, IEEE) received the B.Sc. degree in electrical engineering from Shandong University, Jinan, China, in 2014, and the Ph.D. degree in information engineering from ShanghaiTech University, Shanghai, China, and the University of Chinese Academy of Sciences, Beijing, China, in 2020. He has ever been a Visiting Scholar with the University of California at Berkeley (UC Berkeley), Berkeley, CA, USA, the University of Freiburg, Freiburg im Breisgau, Germany, and Technische Universität Ilmenau (TU Ilmenau), Ilmenau, Germany, during his Ph.D. study. He is currently a Post-Doctoral Researcher with the Laboratoire d'Automatique, École Polytechnique Fédérale de Lausanne (EPFL), Lausanne, Switzerland. His research interests include distributed optimization, robust optimization, and model predictive control, particularly for power and energy systems, cyber-physical system, intelligent transportation, and federated learning.

Yuanming Shi (Senior Member, IEEE) received the B.S. degree in electronic engineering from Tsinghua University, Beijing, China, in 2011. He received the Ph.D. degree in electronic and computer engineering from The Hong Kong University of Science and Technology (HKUST), in 2015. Since September 2015, he has been with the School of Information Science and Technology in ShanghaiTech University, where he is currently a tenured Associate Professor. He visited University of California, Berkeley, CA, USA, from October 2016 to February 2017. His research areas include optimization, statistics, machine learning, wireless communications, and their applications to 6G, IoT, and AI. He was a recipient of the 2016 IEEE Marconi Prize Paper Award in Wireless Communications, and the 2016 Young Author Best Paper Award by the IEEE Signal Processing Society. He is also an editor of IEEE Transactions on Wireless Communications and IEEE Journal on Selected Areas in Communications.

Yong Zhou (Member, IEEE) received the B.Sc. and M.Eng. degrees from Shandong University, Jinan, China, in 2008 and 2011, respectively, and the Ph.D. degree from the University of Waterloo, Waterloo, ON, Canada, in 2015. From Nov. 2015 to Jan. 2018, he worked as a postdoctoral research fellow in the Department of Electrical and Computer Engineering, The University of British Columbia, Vancouver, Canada. He is currently an Assistant Professor in the School of Information Science and Technology, ShanghaiTech University, Shanghai, China. His research interests include 6G, federated learning, and Internet of Things.

Wei Chen (Senior Member, IEEE) received the B.S. and Ph.D. degrees (Hons.) from Tsinghua University in 2002 and 2007, respectively. Since 2007, he has been a Faculty Member with Tsinghua University, where he is currently a Tenured Full Professor and a University Council Member. During 2016-2021, he was the Director of the Degree Office of Tsinghua University. During 2014-2016, he was the Deputy Head of the Department of Electronic Engineering in Tsinghua University. From 2005 to 2007, he was a Visiting Ph.D. Student with the Hong Kong University of Science and Technology. He visited the University of Southampton in 2010, Telecom Paris Tech in 2014, and Princeton University, Princeton, NJ, USA, in 2016. His research interests are in the real-time communication theory. He is a Cheung Kong Young Scholar and a member of the National Program for Special Support of Eminent Professionals, also known as 10,000 talent program. He received the IEEE Marconi Prize Paper Award in 2009 and the IEEE Comsoc Asia Pacific Board Best Young Researcher Award in 2011. He is a recipient of the National May 1st Labor Medal and the China Youth May 4th Medal. He has also been supported by the National 973 Youth Project, the NSFC Excellent Young Investigator Project, the New Century Talent Program of the Ministry of Education, and the Beijing Nova Program. He served as an Editor for the IEEE TRANSACTIONS ON COMMUNICATIONS. He also serves as a standing committee member of All-China Youth Federation and the secretary-general of its education board. He has served as a TPC Co-Chair for IEEE VTC-Spring in 2011 and a Symposium Co-Chair for IEEE ICC and Globecom.

Khaled B. Letaief (Fellow, IEEE) is an internationally recognized leader in wireless communications and networks with research interest in artificial intelligence, big data analytics systems, mobile cloud and edge computing, tactile Internet, 5G systems and beyond. In these areas, he has over 720 papers with over 41,000 citations along with 15 patents, including 11 US inventions. He is a Member of the United States National Academy of Engineering, Fellow of IEEE, Fellow of Hong Kong Institution of Engineers, and Member of the Hong Kong Academy of Engineering Sciences. He is also recognized by Thomson Reuters as an ISI Highly Cited Researcher and was listed among the 2020 top 30 of AI 2000 Internet of Things Most Influential Scholars.

Dr. Letaief is the recipient of many distinguished awards and honors including the 2021 IEEE Communications Society Best Survey Paper Award; 2019 Distinguished Research Excellence Award by HKUST School of Engineering (Highest research award and only one recipient/3 years is honored for his/her contributions); 2019 IEEE Communications Society and Information Theory Society Joint Paper Award; 2018 IEEE Signal Processing Society Young Author Best Paper Award; 2017 IEEE Cognitive Networks Technical Committee Publication Award; 2016 IEEE Signal Processing Society Young Author Best Paper Award; 2016 IEEE Marconi Prize Paper Award in Wireless Communications; 2011 IEEE Wireless Communications Technical Committee Recognition Award; 2011 IEEE Communications Society Harold Sobol Award; 2010 Purdue University Outstanding Electrical and Computer Engineer Award; 2009 IEEE Marconi Prize Award in Wireless Communications; 2007 IEEE Communications Society Joseph LoCicero Publications Exemplary Award; and 19 IEEE Best Paper Awards.

He served as consultants for different organizations including Huawei, ASTRI, ZTE, Nortel, PricewaterhouseCoopers, and Motorola. He is the founding Editor-in-Chief of the prestigious IEEE Transactions on Wireless Communications and has served on the editorial board of other premier journals including the IEEE Journal on Selected Areas in Communications – Wireless Series (as Editor-in-Chief). He has also been involved in organizing many flagship international conferences. From 1990 to 1993, he was a faculty member at the University of Melbourne, Australia. Since 1993, he has been with the Hong Kong University of Science & Technology (HKUST) where he is currently the New Bright Professor of Engineering. While at HKUST, he has held many administrative positions, including the Dean of Engineering, Head of the Electronic and Computer Engineering department, Director of the Wireless IC Design Center, founding Director of Huawei Innovation Laboratory, and Director of the Hong Kong Telecom Institute of Information Technology. Dr. Letaief is well recognized for his dedicated service to professional societies and IEEE where he has served in many leadership positions. These include Treasurer of IEEE Communications Society, IEEE Communications Society Vice-President for Conferences, Chair of IEEE Committee on Wireless Communications, elected member of IEEE Product Services and Publications Board, and IEEE Communications Society Vice-President for Technical Activities. He also served as President of the IEEE Communications Society (2018-19), the world's leading organization for communications professionals with headquarter in New York City and members in 162 countries.

Dr. Letaief received the BS degree with distinction in Electrical Engineering from Purdue University at West Lafayette, Indiana, USA, in December 1984. He received the MS and Ph.D. Degrees in Electrical Engineering from Purdue University, in Aug. 1986, and May 1990, respectively.